International Journal of Engineering Inventions
e-ISSN: 2278-7461, p-ISSN: 2319-6491
Volume 11, Issue 3 [May.-June. 2022] PP: 223-247

A Review on Raman Spectroscopy

Mr. Vikram Singh
Department of Applied Science (Physics)
ITM, An IAMR Group of Institutions Ghaziabad, India

Abstract
Raman spectroscopy is a variety of vibrational spectroscopy that allows the easy interpretation and extremely sensitive structural identification of specimen-based on their unique vibrational properties which is also called fingerprints. Because of continuous technological developments in Raman spectroscopy, the technology has advanced in development and more applications are now possible. This review demonstrates the preponderance of the principal categories of Raman spectroscopy. We present here a general review on theoretical and instrumental Raman technology, as well as its applications throughout many domains. The purpose of the review is to highlight potential applications of many types, particularly those developed to distinguish distinct specimens such as biological, chemical, microbiological, and many others. In this review study, we will focus on Raman spectroscopy applications in the following domain, including theories, instrumentation, popular type Raman Spectroscopy & few application according to current scenario such as in Corona-virus detection & nano-material characterization, and even certain chemical field applications. Raman spectroscopy is a vibrational technique that involves high energy photons based on the inelastic scattering of light in the visible or near-infrared range of the specimen. The wavelength of the preponderance of the scattered light called Rayleigh scattering is the same as that of the laser source light. There are two kinds of light scattering: elastic scattering and inelastic scattering. When the photon frequency does not shift or change wavelength, this is referred to as elastic scattering. Inelastic scattering, which is essential in Raman spectroscopy, is the counterpart. The frequency shift can be utilized to get information about molecular chemistry, biological tissues and many more fields.

Keywords: *Raman Spectroscopy, Coronavirus detection, Raman Surface Enhancement Spectroscopy, Nano-particles, Vibrational Spectroscopy.*

Date of Submission: 01-06-2022 Date of Acceptance: 13-06-2022

---

1. Introduction

This review paper describes the fundamental requirements for Raman scattering based detection technologies. In this review paper, I focused on several spectroscopic phenomena that are pertinent to Raman scattering based detection technologies. All different kinds of Raman scattering phenomena involve changes in laser radiation frequency as a consequence of their interaction with the material. However, because each of these impacts involves a separate set of methodologies and principles, new applications and sensitive data might materialize. I will also provide a brief description of the experimental setup for these various techniques. The intense blue color of the Mediterranean ocean fascinated Indian physicist Chandrasekhara Venkata Raman. He was, however, unimpressed with Lord Rayleigh's explanation that the color of the water was just a reflection of the color of the sky, as described by the classical theory of light scattering for constant frequency in 1871. After much contemplation and considerable effort on a series of measurements of light scattered by liquids as well as some solids, Raman and his group in Calcutta were able to demonstrate in 1928 that the color of the ocean was caused by the scattering of sunlight by water molecules. "However, Adolf Smekal, an Austrian scientist, described the inelastic light scattering phenomena a few years earlier. Photons, according to Smekal, might be dispersed inelastically by molecules in addition to the origin wavelength, shorter and longer wavelengths would be present". Smekal further demonstrated that the frequency shift between incoming and scattered light is caused by the difference in energy between two states of the molecules. Simultaneously, two Russian scientists, Landsberg and Mandelstam, investigated Brillouin scattering from quartz and discovered light scattering with frequency variation. "Furthermore, the finding of Landsberg and Mandelstam was published after Raman's work had been published. Raman was acknowledged to be the first who described the phenomena of the scattering effect of light which was named after him and to do so Sir Raman won Nobel Prize in Physics in 1930". However, the advancement of Raman spectroscopy was rather delayed for a variety of reasons. First, the Raman effect is very weak. Generally, merely Rayleigh is one part in a thousand of the overall intensity of

incoming light dispersed, but Raman scattering reduces this value to one part in a million. Because the Raman effect is so weak, attenuating elastically dispersed light in order to detect in-elastically scattered Raman light is a major challenge. The second reason is that the excitation source in all of the early light-scattering experiments was sunlight, and the materials utilized in the study were liquids. However, these challenges were solved, and things altered significantly with the discovery of the laser in 1960. Thus, the development of laser technology encouraged the conventional field of molecular spectroscopy and Raman spectroscopy in a multitude of ways. The novel laser technology was also the key element in the development of several types of Raman spectroscopes. Today, there are about 25 various varieties of linear and nonlinear Raman spectroscopy methods. The main ones are widely used in fields of chemical science and material science, art restoration, military and medicinal applications, and so on.

Basically, Spectroscopy that was used to study of the interaction between radiation and matter as a function of wavelength. Raman spectroscopy is a branch of vibrational spectroscopy and is a method used to identify the rotational, vibrational and other low-frequency modes of matter that allows an easy interpretation and highly sensitive structural identification of matter. Raman spectroscopy work on a phenomenon known as Raman effect that happens when the electric dipole of matter interacts with the light photon. Raman spectroscopy is a vibrational mode-based technique that involves high energy photons on the inelastic scattering of radiation in the visible or near-infrared region of matter. Scattering is causes of collision between matter particles and light photon, the shift in wavelength is directly proportional to concentration and depends upon the chemical structure of molecular species. Most of the scattered light has the same wavelength as the radiation source known as Rayleigh scattering. Molecules are the composition of two or more bonded atoms that are in continuous motion in the form of either vibrational or rotational or electronic or translational. These different kinds of motion and intermolecular interaction causes different forms of energy possesses in a molecule that can be probed with electromagnetic radiation to get information on molecular structure and composition. A matter molecule may interact with electromagnetic radiation either by absorption or scattering of radiation. Since electromagnetic radiation is quantized and so it possesses discrete energy levels and also matters molecules have discrete energy level. Rotational transitions occur at microwave region, whereas vibrational transitions occur relatively high energy levels such as in the IR, and electronic transitions occur either in the visible or UV region of the EM-spectrum. Stoke Raman scattering happed due to interaction between the ground state matter molecules, so occur far more easily and light photon whereas the anti-stoke Raman scattering arises from interaction of photon and excited state matter molecules. Both Raman and infrared (IR) spectroscopy probe molecular vibrations associated with chemical bonds in a sample to obtain information on molecular structure, composition, and intermolecular interactions. Raman spectroscopy arises from vibrational and rotational motion of molecules happened due to inelastic scattering that depends on nuclear vibrations of matter particles cause a net change in polarizability. Those substances are Raman active may not be IR active, and vice versa and so they will be strong in one effect and weak in other. Since Raman spectroscopy is a nondestructive, reagent less, vibrational spectroscopic technique, it provides rapid molecular characterization of tissue in vivo or in vitro for biopsy, margin assessment, therapeutic evaluation, or laboratory use. It has become common practice today to identify substances, analyze structure and properties of functional molecules, by using Raman spectroscopy**.**

2. Raman Scattering Theory

In this section we will explore the different nature of Raman effects such as Classical nature and Quantum nature. Raman scattering is extremely similar to Rayleigh scattering. In both situations, light is shone on the molecule with enough energy to excite any vibrational or rotational states but not enough to bring it out of its ground electronic state. This radiation then excites the molecule to a virtual state, which decays to lower energy levels. The molecule decay back to its initial state in Rayleigh scattering **Fig. 1(a)** and to a different state in Raman scattering. When the final energy level is greater than the initial state, it is referred to as a Stokes transition whereas when it is lower, it is described as an anti-Stokes transition **Fig. 1(b)**. The light that is emitted during de-excitation will subsequently be examined. Finally, we will look at Raman transitions that are either vibrational or rotational. Raman spectroscopy is a subcategory of vibrational spectroscopy that would be used to identify rotational, vibrational, and other low-frequency modes of materials, allowing for easy interpretation and highly sensitive structural characterization. The Classical Raman effect hypothesis is based on the polarizability of molecules, which represents how effortlessly an electron cloud of a molecule may be deformed by an electric field (light). Smekal's approach provides the foundation of the quantum

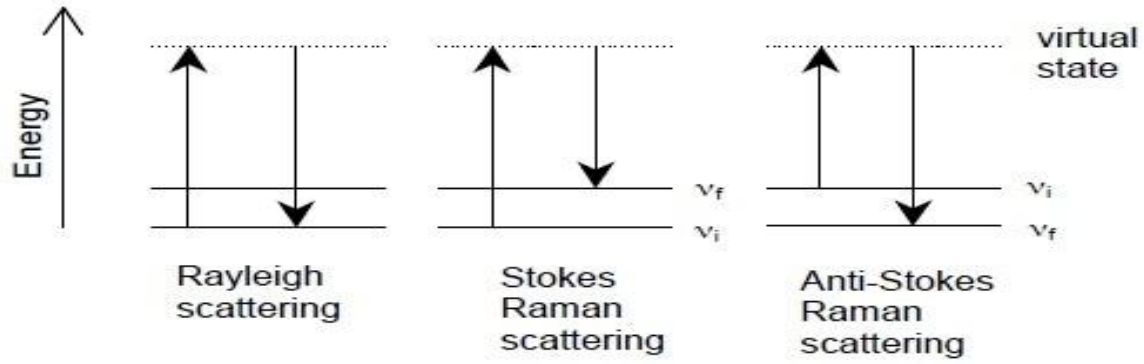

Fig.1: *Energy-level diagram of Rayleigh scattering, Stokes Raman scattering, and anti-Stokes Raman scattering.*

mechanical dispersion (QMD) theory of Raman scattering. This theory provides an expression of the polarizability tensor ($\alpha_{\alpha\beta}$) developed with the help of Kramer's, Heisenberg, and Dirac's time-dependent perturbation theory (KHD**)**. However, since this formalism includes a sum across vibronic states, it is difficult to use in reality. Now let us start to understand one by one the different nature of Raman effects.

2.1. Classical Description of Raman Spectroscopy

The fundamental principle of this spectroscopy is based on a molecule's polarizability and the applied electric field. When a molecule is placed in a uniform electric field, the positively charged nuclei are attracted to the negative pole of the field, while the electrons are attracted to the positive poles, is referred to as polarization. Polarizability is ability of the electron clouds to interact with an electric field. Whenever a beam of high energy electromagnetic radiation strikes with species, the species undergo through oscillating electric dipole moment due to oscillating electric field of interacting radiation beam irrespective of the molecules have permanent dipole moment and so molecular species is said to be polarized usually in state of radiation use high energy laser. "When a photon interacts with a molecule, the electrons and protons move, producing an oscillating dipole. This dipole will then emit photon of different frequencies".

When a photon collides with a molecular species of mass 'M'. Since a molecular species made up of several atoms so every atom have different masses as M_1, M_2 .... etc., displacement represented by x_1, x_2…. and bond strength between these atoms will be K_1, K_2….and so on.

Therefore, the displacement in the atoms will be given by using Hook's Law as follows

$$\frac{M_1M_2}{M_1+M_2}\left(\frac{d^2x_1}{dt^2}+\frac{d^2x_2}{dt^2}\right)=-K_1(x_1+x_2) \quad \text{……..1}$$

$$\frac{M_2M_3}{M_2+M_3}\left(\frac{d^2x_2}{dt^2}+\frac{d^2x_3}{dt^2}\right)=-K_1(x_2+x_3) \quad \text{……..2}$$

and so on

In order to simplified the above expression introduced reduced mass μ_1, μ_2 ….. and displacement considered as q_1, q_2 ... and so

$$\mu_1\frac{d^2q_1}{dt^2}=-K_1q_1 \quad \text{…….……3}$$

and $$\mu_2\frac{d^2q_2}{dt^2}=-K_2\,q_2 \quad \text{.....……4}$$

The wave solution of above-mentioned wave equation is estimated approximately by using wave solution methods

$$q_M=q_{M_0}\cos 2\pi n_k t \quad \text{……...5}$$

Where q_{M_0} be the vibrational amplitude and n_m be the vibrational frequency of modes of the molecular species. For small displacement such as in typical diatomic molecule the polarizability may be expanding in the normal co-ordinates form of Taylor series as

$$\alpha=\alpha_0+\sum_{k=1}^{M}\left(\frac{\partial\alpha_k}{\partial q}\right)_0 q \quad \text{……6}$$

Since the polarizability is the static and sinusoidal oscillating term but to occurrence of Raman scattering, the polarizability be the function of vibration, $\left(\frac{\partial\alpha}{\partial q_M}\right)_0 \neq 0$. In the above mathematical expression the equilibrium position of the atoms are indicated by the subscript '0'.

The frequency of molecular vibration is estimated as

$$n_m=\frac{1}{2\pi}\sqrt{\frac{K_k}{\mu_k}}$$

The electric field associated with beam of light of frequency 'n' be

$$\vec{E} = \vec{E_0} \sin 2\pi nt \quad \text{.....7}$$

Therefore, the induced dipole moment is the product of the polarizability and the electric field associated with beam of radiation

$$\overrightarrow{p_{indu}} = \alpha\vec{E} = \alpha\vec{E_0} \sin 2\pi nt \quad \text{.....8}$$

In above mathematical expression the term "α" called polarizability of the molecular species. The molecular species behaves like as Hertzian oscillator and emit energy in the form of electromagnetic radiation of frequency $'n'$ same as the incident radiation called Rayleigh scattering. Due to so the molecular species has internal motion named either vibrational or rotation.

On substituting values from equation 5,6 into equation 8, we get

$$\overrightarrow{p_{indu}} = \alpha_0 E_0 \cos 2\pi nt + \sum_{k=1}^{M} \left(\frac{\partial \alpha_k}{\partial q}\right)_0 \frac{E_0 q_0}{2} [\cos 2\pi(n_0 + n_k)t + \cos 2\pi(n_0 - n_k)t] \quad \text{.....9}$$

Since as already discussed that molecular species has rotational as well as vibrational motion and so the induced dipole moment due to vibration of molecular species

$$\overrightarrow{p_{indu}} = \alpha_0 E_0 \cos 2\pi nt + \sum_{k=1}^{M} \left(\frac{\partial \alpha_k}{\partial q}\right)_0 \frac{E_0 q_0}{2} [\cos 2\pi(n_0 + n_{osc})t + \cos 2\pi(n_0 - n_{ocl})t]$$

Similarly, the rotation of the molecular species causes induced dipole moment be

$$\overrightarrow{p_{indu}} = \alpha_0 E_0 \cos 2\pi nt + \sum_{k=1}^{M} \left(\frac{\partial \alpha_k}{\partial q}\right)_0 \frac{E_0 q_0}{2} [\cos 2\pi(n_0 + n_{rot})t + \cos 2\pi(n_0 - n_{rot})t]$$

According to Classical Mechanics, an oscillating induced dipole moment emits radiation at the frequency of oscillation $'n_{0'}$. An oscillating dipole emits radiation at the same frequency of the incident light represented by the first term of the above mathematical equation which is known as Rayleigh scattering. The second term of the equation shows the condition of Raman scattering. The oscillating polarizability causes an induced dipole moment that oscillates and emits radiation at frequencies that differ from the incident light.

According to Classical theory of Electrodynamics an oscillating dipole emit radiation of the intensity

$$I = \frac{n_0^4}{12\pi\epsilon_0 c^3} |\vec{p}_{indu}|$$

Therefore

$$I = \frac{n_0^4}{12\pi\epsilon_0 c^3} \alpha_0^2 E_0^2 cos2\pi nt + \frac{n_0^4}{12\pi\epsilon_0 c^3} \sum_{k=1}^{M} \left(\frac{\partial \alpha_k}{\partial q}\right)_0^2 E_0^2 \alpha_k^2 (n_0 + n_k)^4 \cos^2 2\pi(n_0 + n_k)t + \frac{n_0^4}{12\pi\epsilon_0 c^3} \cos^2 2\pi(n_0 - nk)t + \ldots\ldots\ldots \quad \text{.....10}$$

In above expression the first tern represents Rayleigh scattering. In Raman scattering, the molecular species radiates with two frequencies that are modulated by frequency of excited normal vibration. For Stokes Raman Scattering, the Raman scattering radiation has frequency lower as compared of incident radiation and is represented by second term of mathematical expression whereas for Anti-Stokes Raman Scattering frequency of Raman Scattering radiation is higher as compared of incident radiation and represented by third term of above mathematical expression.

Theoretically the ration of intensities of Stokes and anti-Stokes Raman scattering will be

$$\frac{I_{Stokes}}{I_{anti-Stokes}} = \frac{((n_0 - n_k)^4}{((n_0 + n_k)^4} \quad \text{.....11}$$

The classical picture of Raman Scattering does not explain well many aspects of Raman scattering observed experimentally, like the intensities of scattered radiation.

2.2. Quantum description of Raman Scattering

The quantum interpretation of light scattering is different from classical interpretation. Quantum states of material particles are characterized by the help wave function. Quantum mechanically the energy of the system is considered to be discrete. Energy is generally radiated during the transition of the system state from one state to another. At the beginning of the 20th century, electrons were discovered to exhibit diffraction patterns when passed through a double slit in the same manner as light waves do. This experimental evidence has suggested that duality nature that means atomic particles were also wave-like in character, and thus it was reasonable to assume that a wave equation could describe atomic particle behavior. In 1926, Erwin Schrödinger, an Austrian physicist derive a wave equation that represents electron mobility and which evolved to have the same essential

importance in quantum mechanics as Newton's laws of motion have in classical mechanics. The Schrödinger equation defines the shape of the probability waves that govern the mobility of microscopic particles, as well as how these waves are affected by the external fields. In atomic, nuclear, and solid-state physics, this equation is often used. "Nowadays, advanced computational techniques make heavy use of super-computers to solve the Schrödinger equation for different model systems in order to determine the electronic structure of atoms and molecules". The general Schrödinger equation be like

$$\boldsymbol{E\,\Psi = H\,\Psi} \qquad \text{…….. } \mathbf{12}$$

inwhich '**H**' is the total non-relativistic Hamiltonian operator whereas $\boldsymbol{'\Psi'}$ is eigen function and '**E**' is the energy of the system.

Atoms bound by bonds are spatially confined, causing molecular vibrations/rotations to occur at definable energy levels. According to Quantum theory, radiation is considered to be discrete that means radiation is a composition of small particles named Quanta or sometimes also referred as photon having energy $\boldsymbol{hc\vartheta}$ of each photon. When radiation interacts with materials the photon interacts with the material particles. In such kind of interaction have there are three possibilities. The first possibility is that the initial state is maintained by materials particles and photons scattered with original energy. Such interaction is known as Rayleigh scattering and the observed line are said to be Rayleigh lines, interaction referred to be elastic. The second possibility is that the interaction is inelastic in which initially material particle in its ground state with energy $\boldsymbol{E'}$ absorbed energy from a photon and get excited to the higher energy state of energy $\boldsymbol{E''}$, the photon is consequently scattered with less energy $\boldsymbol{hc\vartheta - \Delta E}$, here $\boldsymbol{\Delta E = E'' - E'}$. The result of this get the Raman line with lower frequency than that of incident radiation and such kind of Raman lines are referred to be Stokes lines. This process is said to be Stoke-Raman scattering. The third possibility may be the photon interacts with a material particle at an excited energy state of energy $\boldsymbol{E''}$ and absorbed $\boldsymbol{\Delta E}$ energy from it. In such case materials, particles may be de-excited to the ground state of energy $\boldsymbol{E'}$ and then photon scattered with higher energy $\boldsymbol{hc\vartheta + \Delta E}$. This result in Raman lines of frequency higher than that of incident radiation/light and such Raman lines are said to be anti-stoke lines or anti-stoke Raman lines, the process is said to be anti-stoke Raman scattering. On either side of the Rayleigh line, the Stoke and anti-Stoke Raman lines are symmetrically situated. The Raman shift directly gives the energy difference between the stationary states of the material particles. "A material particle is only said to be Raman active, when the polarizability of a particle (vibration/rotation) changes. In the quantum description, the oscillating electric dipole and polarizability are replaced by a transition electric dipole and polarizability in the quantum description. The transition moment leads to a transition between two quantum states, i and f, only if it is nonzero".

$$\mathbf{M_{ind}(i \rightarrow f) = \left(\frac{\partial \alpha}{\partial Q}\right)_0 \epsilon_0 \int \psi_i Q \psi_f \, dQ \neq 0} \qquad \text{……} \mathbf{13}$$

Here M_{ind} is the moment of Raman transition for a diatomic material particle, ψ_i and ψ_f are wave functions got by the solutions to the time-dependent Schrodinger equation for states i and f, α is the polarizability operator which is a tensor property, ϵ_0 is the electric field amplitude, and Q is the coordinates. Because energy is conserved so the gain in energy $h\vartheta_\vartheta$, by the material particles results in an equal amount of energy hϑ, being removed from the incident photon, where incident energy is $h\vartheta_0$. This change in energy is the energy of a scattered photon **[19]** is given by

$$\mathbf{\Delta E = h(\vartheta - \vartheta_0) = h(\vartheta_0 - \vartheta_\vartheta)} \qquad \text{……} \mathbf{14}$$

Radiation is emitted at longer wavelengths (lower energy) than incident light because the wavelength is inversely proportional to frequency.

As shown in **Fig. 2**, when a molecule is initially excited before to irradiation with $\boldsymbol{E_1 = \frac{3}{2} h\vartheta_\vartheta}$ and is promoted to a virtual energy level, it eventually relaxes to the ground state with $\boldsymbol{E_0 = \frac{1}{2} h\vartheta_\vartheta}$ after scattering. Hence final energy state of the material particle will be $\boldsymbol{E_0 = E_1 - h\vartheta_\vartheta}$, here the particles of the material released energy. This correlates to photon energy, $\mathbf{h = h\vartheta}$, being transferred to the incident photon's energy . The energy of the scattered photon will be $\boldsymbol{h(\vartheta_0 + \vartheta_\vartheta)}$. Therefore, Radiation with shorter wavelengths (greater energy) than the initial radiation is emitted. However, because Stokes-shifted line is more intense than anti-Stokes line, it is usually measured. Because no actual energy levels are involved in conventional Raman spectroscopy, the result is wavelength-independent (only virtual states).

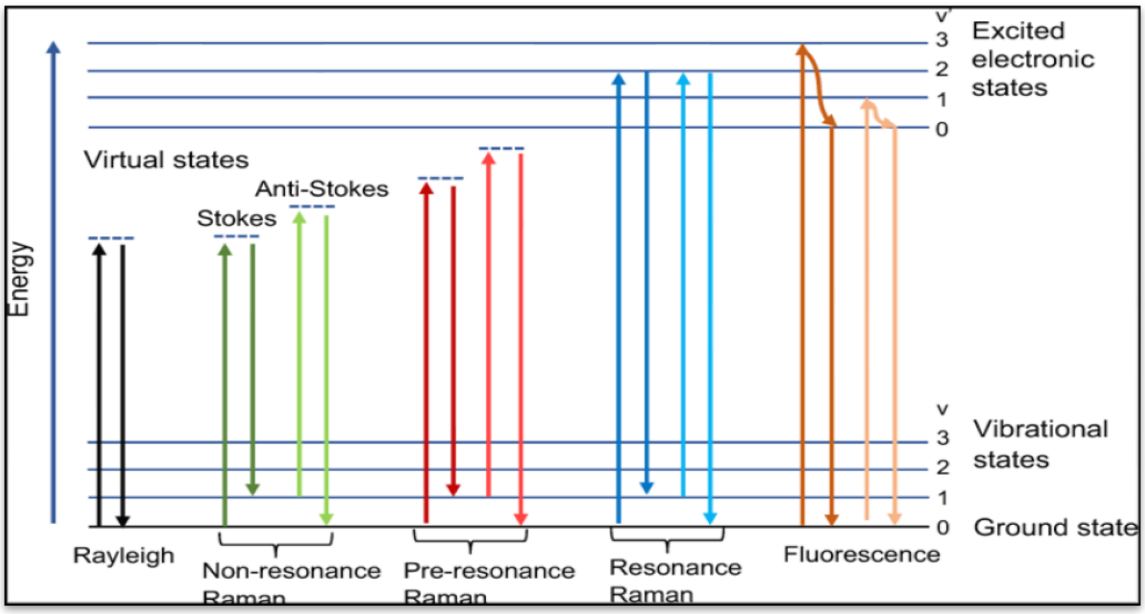

Fig. 2: *Rayleigh scattering, Raman scattering, and fluorescence energy level diagram*.

This is known as non-resonance Raman. In resonance Raman spectroscopy, a variety of conventional Raman, atomic vibrations are monitored in a wavelength-dependent approach. A resonance effect is observed when the wavelength of the exciting source aligns with an electronic transition of the molecule, and the strength of some Raman-active vibrations can be enhanced by a factor of $10^2 - 10^6$. Before a photon is emitted, molecules are excited to a virtual energy level for a small amount of time, on the range of picoseconds, in the Raman effects.

2.3. Born–Oppenheimer approximation

The Born-Oppenheimer concept is one of those excellent approximations that, even when it fails, served as a basis for deliberation and systematic improvements. The Born-Oppenheimer approximation is one of the fundamental ideas enabling the characterization of molecular quantum states. There would be no molecular structure, solid-state crystal structure, molecular vibrations, phonons, electronic band structure, and so on if the Born-Oppenheimer approximation did not exist as a foundation because the Born-Oppenheimer approximation permits for the decoupling of electronic and atomic mobility. The Born-Oppenheimer approximation recognizes the huge difference in electron mass and atomic nuclei masses, as well as the time scales of their mobility. When characterizing the electrons in a molecule, the Born-Oppenheimer approximation excludes the motion of the atomic nuclei. The Born-Oppenheimer approximation has a physical foundation in the fact that the mass of an atomic nucleus in a molecule is massively larger than the mass of an electron (more than 1000 times) because of this asymmetry, nuclei move significantly slower than electrons and can be considered as stationary while the electrons move around them. The solution of the Schrödinger equation for a single particle is elementary, but for many-body systems, it is a daunting undertaking. Without the Born–Oppenheimer approximation, it is impossible to distinguish the entire wave function into an electronic and a nuclear component in many-particle systems. As a result, rather than trying to solve the Schrödinger equation for all particles at the same time, it is possible to consider the nuclei to be stationary in a place and solve the Schrödinger equation for the electrons in the stationary electric potential originating from the nuclei. Then by invoking approximation the entire wave function may be differentiated into two components, corresponding to the nuclear and electronic wave functions.

The electronic Schrödinger equation is

$$\hat{\mathbf{H}}_{\mathbf{elec}}\boldsymbol{\varphi}_{\mathbf{elec}} = \hat{\mathbf{E}}_{\mathbf{elec}}\boldsymbol{\varphi}_{\mathbf{elec}} \qquad \text{.....15}$$

Further, the electronic wave function may be written in the electronic co-ordinates and parametrically of nuclear co-ordinates as $\boldsymbol{\varphi}_{elec} = \boldsymbol{\varphi}_{elec}(\boldsymbol{r}_i; \boldsymbol{R}_\alpha)$.

"The Hamiltonian for the stable set of location $\boldsymbol{R}_\alpha$ of the nuclei may be given by

$$\hat{\boldsymbol{H}}_{elec} = -\sum_{i=1}^{n}\frac{\mathbf{1}}{\mathbf{2}}\nabla_i^2 - \sum_{i=1}^{n}\sum_{\alpha=1}^{N}\frac{\boldsymbol{Z}_\alpha}{\boldsymbol{r}_{i\alpha}} + \sum_{i=1}^{n}\sum_{j>i}^{n}\frac{\mathbf{1}}{\boldsymbol{r}_{ij}}$$

Here 'n' represents the total number of electrons in the domain of 'N' electric potential. The first component of the above-mentioned equation is the operator for electron kinetic energy, the second term reflects the Coulomb attraction among electrons and nuclei, while the last component indicates electron repulsion".

3. Instrumentation

A Raman spectrometer is composed of several components such as a light source, a mono-chromator, a specimen container, and a sensor. **Fig.3** The block diagram demonstrates the equipment required to achieve a Raman spectrum, which includes a source of high-intensity monochromatic light, a specimen that does not require any special preparedness (gas, liquid, or solid), a double mono-chromator (filter) to ignore stray light, and a charge-coupled device (CCD) detector, which is mostly used for Raman spectroscopy. *Ex-vivo ("outside of a living body")* applications are generally performed using Raman instruments designed for laboratory research. These systems, constructed for investigation and treatment, are usually designed to gather high-quality spectra with the ability to determine and adjust experimental parameters by using multiple excitation/detection wavelengths and data collecting periods. These systems are also utilized in the development and test statistical algorithms/models for material/tissue categorization. For *in vivo ("within the living")* clinical applications, a small footprint of high-resolution equipment with instantaneous measurement is essential. In most cases, a Raman fibre optic probe is mostly used for access to organs because when compared to laboratory research-grade equipment, the smaller footprint may indicate weaker resolution or a smaller spectrum range of observation. The term weaker resolution implies that information may be lost and spectral characteristics may be difficult to differentiate. Lasers are exploited as photon sources in modern Raman spectrometers because of their extremely monochromatic nature and tremendous beam intensity. Because the Raman effect is low, the Stokes lines are approximately 1000 times shorter than the Rayleigh scattered components. Raman spectrometers in the visible spectral range utilize filters to extract the signal from a relatively limited range centered on the frequency corresponding to laser light. Light scattering Raman spectroscopy and Fourier Transform Raman Spectroscopy vary enormously between laser sources and Raman scattering detection methods. Both methodologies have tangible advantages, and the technique that best fits the sample should be chosen. Furthermore, conventional Raman spectrometer to material characterization includes the microscope to concentrate the laser beam to a narrow spot, have a diameter of about 1-100mm. Raman spectroscopy uses laser light at a number of wavelengths in the ultra-violet UV (325nm), visible (780nm, 633nm, 532nm and 473nm) and in the near infrared (1064nm) regions of the spectrum. Several types of lasers can be used as the excitation source, like krypton ion (530.9 and 647.1 nm), He: Ne (632.8 nm), Nd: YAG (1064 nm and 532 nm) argon ion (488.0 and 514.5 nm), and diode laser (630 and 780 nm). The introduction of a near-IR (NIR) excitation laser at 1064 nm provides a lesser fluorescence effect than visible wavelength lasers. The introduction of a near-IR (NIR) excitation laser at 1064 nm provides a lesser fluorescence effect than visible wavelength lasers.

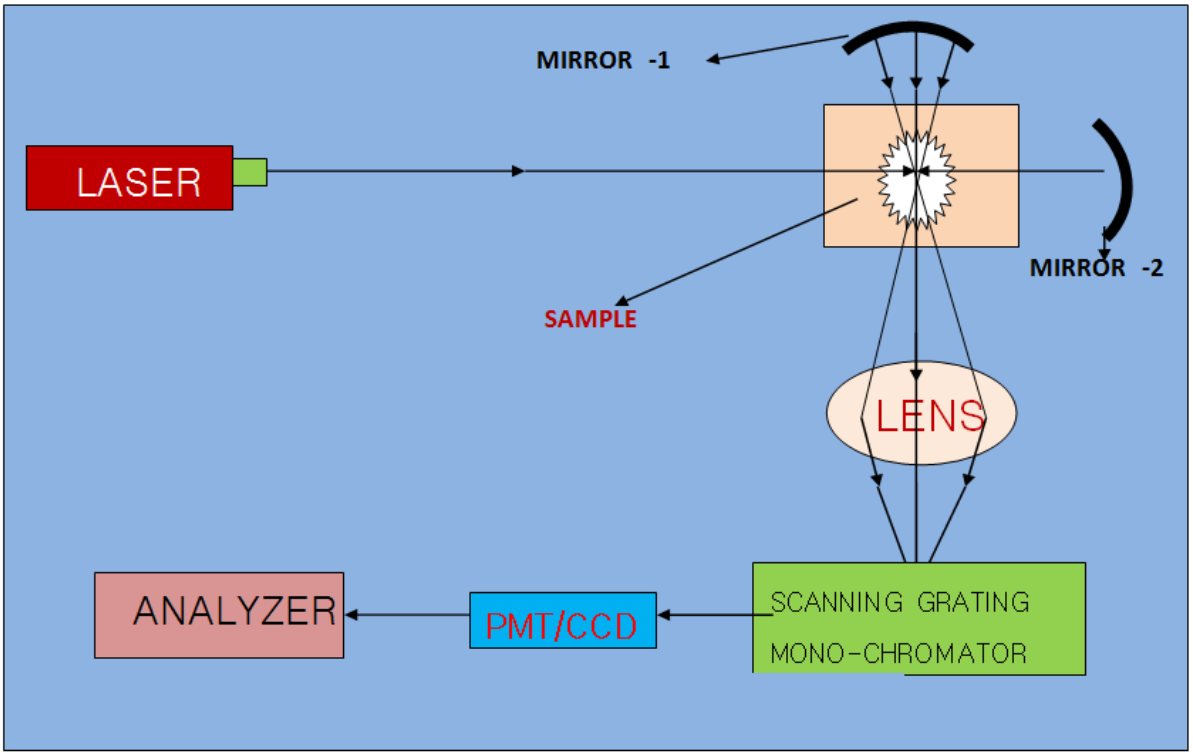

Fig.3: *Raman Spectrometer block diagram.*

Hand-held Raman spectrometers are commercially available. The SciAps ReporteRt (previously DeltaNu, Inc.), the Snowy Range Instrument CBEXt, the Thermo Scientific First Defendert (formerly Ahura, Inc.), and the B&W TEK NanoRamt are among these spectrometers. When combined with optical fibres, Raman spectroscopy provides the additional advantage of remote sensing. The optical fibres are in charge of transporting Raman signals by collecting scattered photons. The fibre optic module includes fibres that transport the laser excitation along with one fibre and the scattered radiations to the detector via other fibres. The primary challenge of Raman spectroscopy is distinguishing the weak Raman signal from Rayleigh scattering and random light, which appear prominently in the neighborhood of the laser wavelength. This is accomplished by using a notch filter to cut out the spectral region around the laser wavelength. Raman spectroscopy has been implemented in real-time monitoring systems to identify illicit narcotics, hazardous material in the environment, and chemical and biological warfare weapons.

Fig 4 shows, a typical laboratory Raman system's configuration. A long pass edge filter (or notch filter) reflects laser light, which is then directed via lens 1 to refocus the laser light onto the sample. In a 180° backscatter geometry, lightly scattered off the sample is collected.

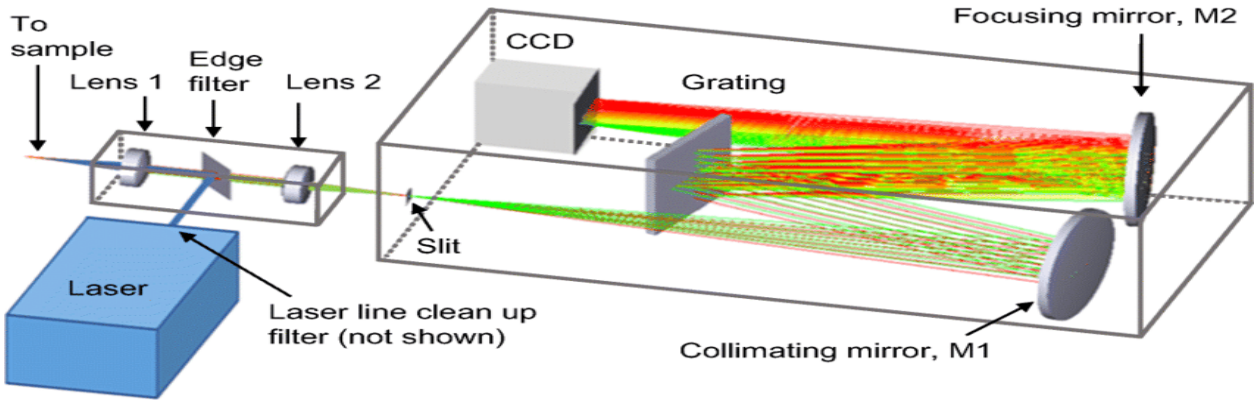

Fig.4: *A laboratory Raman system's configuration.*

Lens 1 collects light, which is directed to an edge filter, which inhibits laser light while allowing Raman scattered light to pass through. Mirror M1 collimates the light entering the slit and directs it onto the spectrometer's grating. The grating scatters the light focused by mirror M2 into representations of the charge-coupled devices entrance slit (CCD).

4. Description of Popular Raman Technologies

4.1. Coherent Raman Spectroscopy(CRS)

CRS (coherent Raman scattering) refers to a specific kind of light-matter interaction. Despite predictions made as early as the 1930s, coherent light scattering events involving multiple incoming photons concurrently interacting with the scattering medium were not seen until laser sources became accessible in the 1960s. In 1961, the first laser-based Raman scattering experiment was performed. The techniques of stimulated Raman scattering (SRS) and controlled Raman scattering (CARS) have become popular four-wave mixing techniques. The unique method in which the material responds to the incident light fields is essential to this kind of interactions: the reaction provides information about material oscillations at different frequencies of two incident light domains. As a consequence of expressing the light field frequencies ω_1 and ω_2 the coherent Raman interaction is dependent on oscillatory movements in the material at the frequency $\Omega = \omega_1\text{-}\omega_2$. CRS methods, as compared to spontaneous Raman scattering, may provide significantly stronger vibrationally sensitive signals. CRS techniques, in general, provide more comprehensive control of the medium's Raman response than spontaneous Raman approaches. The Raman vibrational response is governed by molecular coherences, which may be probed more directly with CRS. CRS techniques can resolve the ultrafast development of such Raman coherences on the proper timeframe when ultrafast pulses are employed. CRS methods also provide more comprehensive molecule orientation information than spontaneous Raman techniques. Furthermore, advanced resonant Raman (coherent or spontaneous) methods may investigate the material's electrical and vibrational characteristics selectively, providing access to numerous molecular data.

4.2. Coherent Anti-Stoke Raman Spectroscopy(CASRS)

Maker and Terhune were the first to demonstrate a spectroscopic method based on coherent anti-Stokes Raman scattering (CARS) in 1966. CARS spectroscopy is a potential method that has been widely used in interdisciplinary study disciplines such as biology, chemistry, physics, healthcare, defence, remote sensing,

forensics, and material science. Recent state-of-the-art breakthroughs include the detection of bacterial spores, application of coherent Raman microscopy, gas-phase thermometry of reacting and non-reacting flows, and many more. CARS involve the interaction of four waves designated as pump (p), Stokes (s), probe (p') and anti-Stokes (CARS) where pump and probe are usually fixed to the same frequency ($\omega_p = \omega_{p'}$). CARS enable chemical selectivity attributable to resonant amplification of the third-order nonlinear signal if the difference in frequency between the pump and Stokes waveforms satisfies the sample's vibrational transition Ω_r (i.e.$\Omega_r = \omega_p - \omega_s$). CARS is nonlinear optical process of a third order. CARS have a better signal-to-noise ratio because of its greater conversion efficiency, the fact that the signal is produced as a collimated beam, and the lack of a big mono-chromator. The advantage of the spontaneous Raman effects over the signal to noise ratio can be ten orders of magnitude. The signal levels in the CARS case are on the order of 10^{10} photons per second or higher, so even if the non-resonant background level is a 100 times larger than the CARS signal, it could theoretically be subtracted and still abandon a signal to shot noise ratio of at least 1000:1. The square of the power at the pump frequency ω times the power at the Stokes frequency $\omega - \Delta$ determines the peak signal intensity in a CARS spectrum. This means that pulsed lasers with high peak power, and thus also strong signals, may be used with low average power pulsed lasers. CARS have the same information content as Raman spectroscopy since it is a coherent spectroscopy. The key distinction is that CARS is a four-wave mixing process that produces a coherent collimated directed beam with many orders of magnitude more intensity than the pump and Stokes beams, and the wavelength is blue-shifted in comparison.

4.3. Surface-Enhanced Raman Spectroscopy (SERS)

Surface-enhanced Raman spectroscopy (SERS) is one of the most sensitive devices, allowing for extremely sensitive structural detection of low concentration analytes via the amplification of electromagnetic fields engendered by the excitation of adsorbate molecules' localized surface plasmons (LSP) on the roughened surface of the metal. Fleischmann and colleagues published the first article describing the strong Raman signal from the interface in 1974. According to the authors, the high-intensity signal is due to the enormous number of adsorption sites on the roughened surface. In 1977, the groups of Jeanmaire, van Duyne, Albrecht, and Creighton demonstrated that the increased intensity of the Raman signal is due to a significant increase of the Raman cross-section of the adsorbed molecules, a technique known as surface-enhanced Raman spectroscopy. There are two widely recognized hypotheses that have been established and demonstrated by several researchers. The first one is electromagnetic (EM) enhancement and the other is chemical enhancement. In any case, samples are typically placed on a nano-structured metallic substrate, known as SERS substrate, where the enhancement occurs due to the interaction between the incoming light, the target sample molecule and the metallic surface. SERS is one of the most sensitive instruments, capable of detecting analytes at extremely low concentrations. The SERS approach is based on particle enhancement of the scattered Raman signal on the surface of the metal. The consequence of electromagnetic waves interacting with metal in the process known as plassmon resonance is signal amplification. SERS is distinguished by a significant increase in the cross-section for the analyte's Raman scattering, up to 15 orders of magnitude more than the conventional Raman technique. In the SERS technique, the gain in signal intensity may even be 10^6 times greater than with conventional Raman spectroscopy. Noble metal nanostructures, such as silver and gold, are popular examples of SERS substrates because they lack Raman active modes. Excitation of localized surface plasmon resonance (LSPR) modes of metallic nanostructures occurs at the resonance frequency of the incoming light, resulting in EM amplification.

Localized dipoles are formed under these conditions, resulting in an enhancement in the localized electric field surrounding the metal nanostructure (**Fig.5**). The size of such induced dipoles is determined by the intensity of the input electric field (E_{ind}) and the polarizability of the metal structure (α_{metal}). The amplified localized electric field surrounding the metal nanostructure subsequently interacts with the specimen at the metallic surface, resulting in another induced dipole in the specific specimen. The stimulated dipole in the target molecule may have three dipole subsystems: a dipole with a comparable angular frequency (ω_{inc}) to the incident EM radiation and a second subsystem with a slightly lower angular frequency ($\omega_{inc}-\omega_{vib}$) relative to the incident EM radiation, whereas the third component with slightly higher angular frequency ($\omega_{inc}+\omega_{vib}$) relative to incident EM radiation, The difference in angular frequencies in the last two components is proportional to the molecule's vibrational energy. These three components correspond to the Rayleigh, Stokes, and anti-Stokes scattering, respectively. To acquire such a high gain, the particles must be absorbed on or near the surface of the metal substrate (approximately 10 nm).

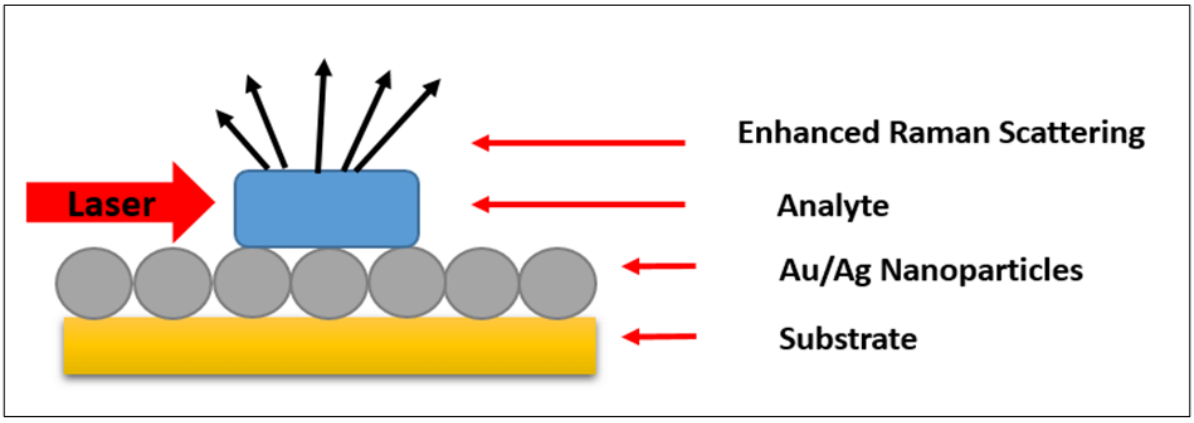

Fig.5: *Raman scattering system with surface enhancement*.

4.4. Fourier Transform Raman Spectroscopy(FTRS)

FTIR is an absorption spectroscopy method that involves the passing of mid-infrared light through a material. While certain wavelengths are absorbed, some other else passes through the sample unaffectedly. The aim of absorption spectroscopy, in general, is to determine how well a material absorbs or transmits light at various wavelengths. Although absorption and emission spectroscopy are substantially different, they are closely connected in operation, with every approach for emission spectroscopy also being applicable to absorption spectroscopy. Fourier-transform spectroscopy is a measuring technique that collects spectra based on measurements of a radiation source's coherence utilizing time-domain or space-domain measurements of electromagnetic or other kinds of radiation. It can be used in optical spectroscopy, infrared spectroscopy (FTIR, FT-NIRS), nuclear magnetic resonance (NMR) and magnetic resonance spectroscopic imaging (MRSI), mass spectrometry, and electron spin resonance spectroscopy, among several other forms of spectroscopy. A Systematical diagram of Fourier Transform Raman Spectroscopy is illustrated in **Fig.5**. The terminology Fourier-transform spectroscopy derives from the fact that all of these methodologies require a Fourier transform to transform raw data into the real spectrum, which is based on the Wiener–Khinchin theorem in many situations in optics involving interferometers. Characterizing the spectrum of a light source, or how much light is emitted at each distinct wavelength, is one of the most fundamental jobs in spectroscopy. Passing light through a mono-chromator, a device that blocks all light save that at a certain wavelength, is the most basic instrument to determine a spectrum. The use of Fourier-transform spectroscopy to obtain the get knowledge is less obvious. Rather than permitting only one wavelength to flow through to the detector at a time, this approach allows a beam containing several wavelengths to pass through at the same time and detects the overall beam intensity. The needed processing is a standard algorithm known as the Fourier transform, thus the term "Fourier-transform spectroscopy".

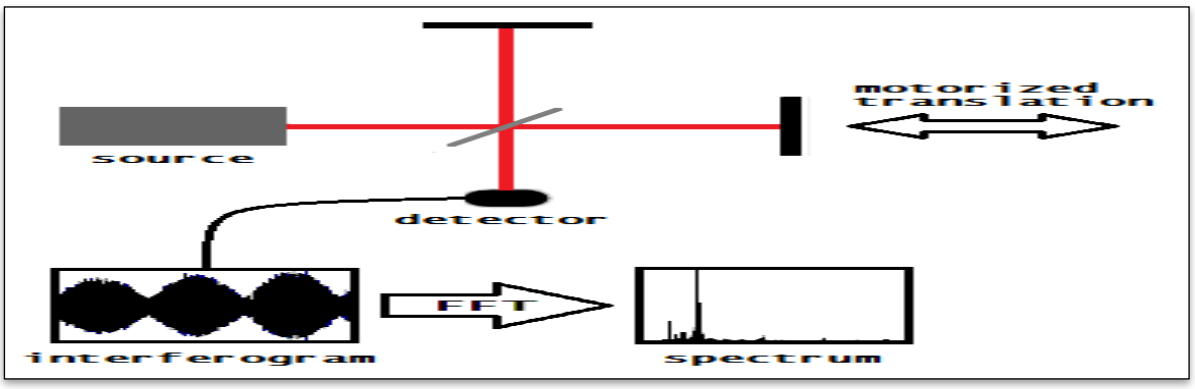

Fig. 6: *Systematical diagram of Fourier Transform Raman Spectroscopy*.

The extraction of the spectrum is done as follows. The intensity in the interferometer $\boldsymbol{p}$ and wave-number $\boldsymbol{\vartheta} = \frac{\mathbf{1}}{\boldsymbol{\lambda}}$ as a function of the path length difference is

$$I(p, \vartheta) = I(\vartheta)[1 + cos2\pi\vartheta p]$$

Here $I(\vartheta)$ is the spectrum that has to be identified. It's worth noting that the sample does not have to modulate $I(\vartheta)$ before the interferometer. In reality, most FTIR spectrometers position the sample in the optical path after the interferometer. The detector's overall intensity is

$$I(p) = \left(p \int_0^\infty I(p,\vartheta)\, d\vartheta\right)$$

$$I(p) = \left(p \int_0^\infty I(\vartheta)[1 + cos2\pi\vartheta p]\, d\vartheta\right), \text{ for all the value of 'p'.}$$

4.5. Hyper Raman Spectroscopy(HRS)

Absorption, emission, and scattering can emerge when substances interact with incident radiation, necessitating transitions among molecular (electronic, vibrational, and rotational) states of the system. Light scattering phenomena associated with vibrational transitions within the electronic (ground) state of the molecule are referred to as the vibrational Raman effects. Generally, the scattered photons in Raman scattering (RS) are Stokes or anti-Stokes shifted due to the difference in energy between both the initial and final vibrational modes (**as shown in Fig. 7a**), in the two-photon excited process of hyper Raman scattering (HRS), the scattered radiation occurs near the second harmonic of the excitation wavelength (**as shown in Fig. 7b and 7c**). When a sufficiently intense electric field is applied, HRS as a non-linear process becomes significant.

The number of hyper Raman Stokes photons produced per second n^{HRS} by the annihilation of two photons at the frequency ϑ_0 and the production of a photon at the frequency$2(\vartheta_0 - \vartheta_k)$ (**Fig. 7b**) may be written as

$$n^{HRS} = \sigma^{HRS} n_0^2$$

$$\sigma^{HRS} \alpha \ \langle |\beta_{if}|^2 \rangle$$

Here n_0 is excitation intensity in photons per cm^2 per second, σ^{HRS} is HRS cross section whereas the transition hyper polarizability involved with the chemical transition between both the initial and final states is denoted by β_{if} . The modeling of HRS spectra entails determining the vibrational frequencies and normal modes, calculating the hyper polarizability and its derivatives, and averaging suitable orientations based on the illumination–observation geometry.

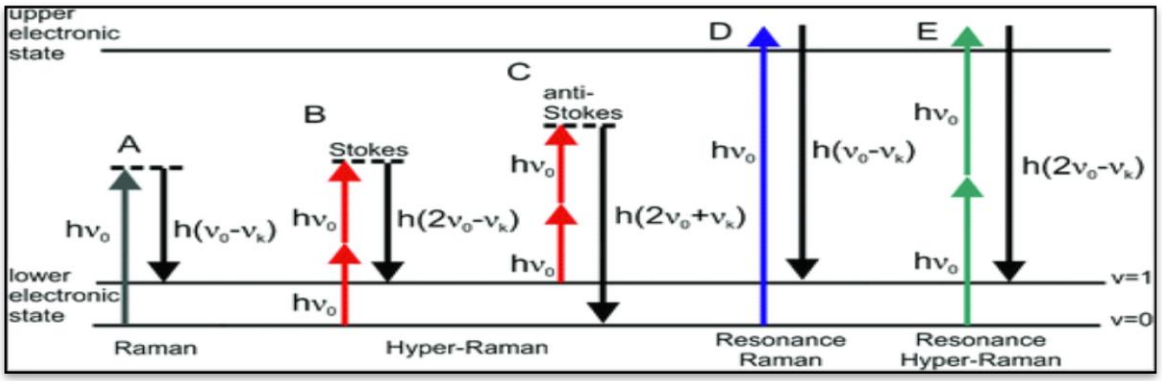

Fig.7: *Schematic representation of vibrational:* ***(a)*** *linear Stokes Raman scattering,* ***(b)*** *Stokes hyper Raman scattering,* ***(c)*** *anti-Stokes hyper Raman scattering,* ***(d)*** *Stokes resonant Raman scattering,* ***(e)*** *Stokes resonant hyper Raman scattering. In each case, the atomic system goes through a vibrational transition from the initial state (v = 0 for Stokes and v = 1 for anti-Stokes) to the final state (v = 1 for Stokes and v = 0 for anti-Stokes), which is associated with the normal mode k and the accompanying frequency nk. Both vibrational states are electronic ground states*.

4.6. Surface-Enhanced Hyper Raman Spectroscopy (SEHRS)

Surface-enhanced hyper Raman scattering spectroscopy is focused on detecting extremely strong hyper Raman signals whenever the scattering molecule is in close contact to nanoparticles. Surface-enhanced hyper Raman scattering is just an inelastic sum of frequency scatted by two photons, whereas normal Raman scattering is caused by a single photon. SERS total surface enhancement factors are predicted to be in the range of 10^{14}. The amplification might be caused by molecule electronic resonance, in which the chemical transition coincides with the sum frequency of the incoming photons. When both the surface effect and the resonance effect are applied simultaneously, the surface enhancement for hyper-Raman scattering is maximized. The majority of SEHRS studies were carried out at 1064 nm excitation employing mode-locked Nd: YAG lasers or Q-switched laser beams. Van Duyne's group gave the first description of SEHRS spectra combining experiment and theoretical study for vibrational assignment, in 1988. It was also observed that compressing the signal to just a few picoseconds can enhance the strength of SEHRS. SEHRS has also been explored for biological applications. The Kneipp group conducted an early research in which they exploited SEHRS to record the stretches of biological bonds such as amide I and III and the C-O bond in DNA**.** SEHRS may also be used to investigate the

electrochemical reactions on electrode surfaces**.** The experimental studies demonstrated that SEHRS may be exploited as a possible ultrafast technique to examine the dynamics of complicated reactions with sensitivity greater than that of SERS. Furthermore, SEHRS may be exploited to examine excited states, as proven by the Camden group. By using unique second-order nonlinearity multi-photon plasmonic enhancement and intrinsic frequency doubling will afford SEHRS an advantage in being recognized in the categories of valuable detection methodology.

4.7. Resonant Raman Spectroscopy (RRS)

Resonance Raman spectroscopy (RRS) is a sophisticated technique for studying vibrational bands in the group frequency range, and the information gained is comparable to that provided by Fourier transforminfrared (FTIR) and Raman experiments. A Schematic illustration of Infrared, Spontaneous and resonance Raman transition is shown in **Fig.10**. RRS improves spontaneous Raman by a factor of 10^6 to 10^8. RRS involves use of a laser light with a frequency near to the energy necessary for a compound's electronic transition. The intensity of Raman scattering is increased by this resonance in frequency between the incident light and the analyte. In **Fig. 8** demonstrates the differences between IR, spontaneous Raman, and resonance Raman spectroscopy methodologies.

In RRS, the resonance effect is caused by the coupling of the molecule's vibrational transition with the mobility of electrons associated with the electronic excitation. RRS enhances sensitivity, allowing the material to be detected at micro-molar concentrations, whereas FTIR and traditional Raman need milli-molar concentrations. The limitation of this study is that the laser light used for excitation might destroy the sample; however, this can be mitigated by agitating the sample or utilizing flow methods. RRS is classified into visible RRS (VRRS) and ultraviolet RRS (UVRRS) depending on what kind of bond present in the sample. RRS has been used to investigate conformational changes in chromo-phores' photoproducts.

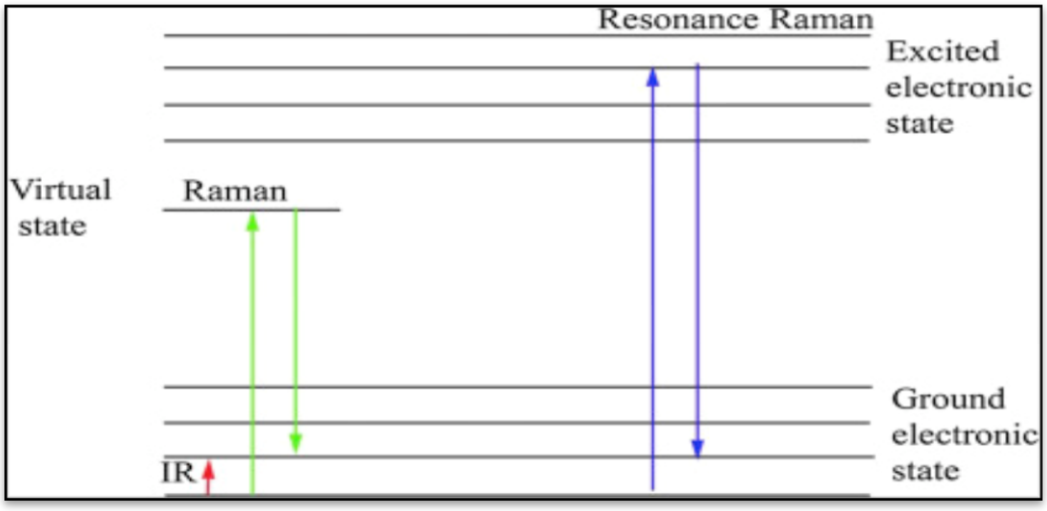

Fig.8: *Schematic illustration of Infrared, Spontaneous and resonance Raman transition*.

4.8. Resonance Hyper-Raman spectroscopy(RHRS)

Resonance hyper-Raman spectroscopy is a modification of resonance Raman spectroscopy wherein the purpose is to accomplish a two-photon absorption excitation to a certain energy level in the target molecule of the sample. Two photons are absorbed into a molecule at the same time in two-photon absorption. Only one photon is released when the molecule recovers from its excited state to its initial state. This is a distinctive kind of fluorescence. Certain portions of molecules can be targeted in Resonance Raman spectroscopy by synchronizing the wavelength of the incident laser beam to the "color", energy between two desirable electron quantum levels of the component of the molecule being examined. This is known as resonance fluorescence, which is why the name "Raman spectroscopy" includes the term "resonance." Single or double photon absorption can be used to achieve some excited states. However, in certain circumstances, double photon excitation may be performed to estimate more information about excited states than single photon absorption. Both resonance Raman and resonance hyper Raman spectroscopy have various limits and consequences. Resonance Hyper Raman spectroscopy, may excite atoms to emit light at wavelengths beyond the laser's adjustable range, therefore expanding the range of molecule components that can be stimulated and analyzed. The resonance hyper Raman spectroscopy is a variety of "non-linear" Raman spectroscopy. When a photon is emitted and the electron cloud relaxes back to its initial state in linear Raman spectroscopy, the amount of energy that passes

into the excitation of an atom is the same amount that exits the electron cloud of that atom when a photon is released. The phrase "non-linear" refers to the fact that emission energy is lower than input energy. In another way we can say that the energy entering the system no longer equals the energy leaving it. Because the energy input in hyper-Raman spectroscopy is significantly higher than in traditional Raman spectroscopy.

5. Clinical Application of Raman Spectroscopy

Over the last few decades, a number of research groups have investigated at the therapeutic potential of Raman spectroscopy, and they continue to uncover new medical issues for which the remarkable sensitivity of Raman scattering offers tremendous promise. Clinical research have been used various implementations of the devices mentioned above to illustrate the potential of Raman spectroscopy to affect medical treatment. We offer a review of major (n>50) clinical in vivo research focusing on the use of Raman spectroscopy for illness diagnosis and sensing in this part project report. These project reports offer a glimpse about where the field is in terms of clinical use of this technique (**Table 1**). Cancer is perhaps the most common clinical target studied with Raman spectroscopy. Large clinical trials have been ongoing in a variety of organ systems, all of which share the following characteristics: a need for better early detection with high sensitivity and specificity, well-characterized disease processes, and relative ease of access to the organ under research. The tools used in these investigations vary significantly, but the anatomical target of interest is at the heart of all of them. It's also worth noting that all significant clinical studies published to date have been carried out by the same few research organizations, indicating the necessity for further research to extend the reach of Raman spectroscopy to in vivo human investigations (**Table 1**).

Table 1: *Overview of large clinical studies (n > 50) performed with Raman spectroscopy in vivo in humans*

Disease type	Raman method	Group	Publication year	Patient number	Sensitivity (%)	Specificity (%)	Ref.
Barrett's esophagus	Probe Raman	Wilson et al.	2005	65	86 (dysplastic), 88 (high grade)	88 (non2splastic), 89 (non-high grade)	82
Barrett's esophagus	Confocal Raman	Huang et al.	2014	373	87 (high grade)	84.7	101
Cervical cancer	Probe Raman	Murali Krishna et al.	2014	63	100	96.7	162
Cervical cancer	Probe Raman	Murali Krishna et al.	2014	93	100	93	161
Cervical precancer	Confocal Raman	Huang et al.	2013	84	81 (dysplasia)	87.1	163
Colon cancer	Probe Raman (HF)	Huang et al.	2015	50	90.9 (adenoma)	83.3 (hyperplastic polyps)	128
GI cancer	Probe Raman	Huang et al.	2011	107	92.6 (gastric) and 90.9 (esophagus)	88.6 (gastric) and 93.9 (esophagus)	99
GI cancer	Probe Raman	Huang et al.	2014	450	81.3 (prospective)	88.3	186
GI ulcers	Probe Raman	Huang et al.	2010	71	82.1 (malignant ulcers) 84.7 (benign ulcers)	90.8	187
Oral cancer	Probe Raman	Murali Krishna et al.	2012	104	86 (tumors) 72 (pre-malignant)	74	176
Oral cancer	Probe Raman	Gupta et al.	2014	199	96 (malignant)	99 (normal)	180

					88 (premalignant), 84 (malignant) (multiclass)	77 (multiclass)	
Oral cancer	Probe Raman	Murali Krishna et al.	2013	84	92.7 (tumor)	98.7 (healthy control) 84 (contralateral normal)	177
Skin cancer	Probe Raman + fluorescence	Tunnell et al.	2014	76	100 (malignant melanoma) 90 (non-melanoma cancer)	100 (pigmented lesion) 85 (normal)	154
Skin cancer	Probe Raman + fluorescence	Moryatov et al.	2014	50	89 (malignant melanoma)	87	173
Skin cancer	Probe Raman	Meinke et al.	2015	104	74 (basal + squamous cell)	82	172
Skin cancer	Probe Raman	Zeng et al.	2012	453	90 (cancer vs. benign)	64	6
Skin cancer	Probe Raman	Zeng et al.	2008	289	91 (cancer) 97 (malignant melanoma)	75 (benign) 78 (pigmented lesion)	174

5.1. Cervix Cancer

Cervical cancer is a largely preventable illness because the transition from pre-cancer (or dysplasia) to cancer takes a long time, allowing for a large diagnostic and treatment window. Cervical cancer rates have dropped substantially in developed nations as a result of aggressive screening program. Cervical cancer is one of the most prevalent causes of cancer-related mortality among women, accounting for about 90% of the 2,65,000 cervical cancer deaths globally in underdeveloped countries where limited resources prohibit comprehensive screening. Over the last two decades, Raman spectroscopy has been studied as an early diagnostic technique for cervical malignancies and pre-cancers. In vivo, our team showed that Raman scattering could detect normal, benign, low-grade, and high-grade dysplastic tissues. Diagnostic accuracies of up to 88% were attained by combining analytical algorithms with data gathering. Further research revealed that adding hormonal/menopausal status increased the prediction accuracy to 94%. Cervical inflammation, parity status, and body mass index have been discovered as new variables to consider, although other patient characteristics such as race/ethnicity and socioeconomic position have been found to have a modest impact on Raman scattering-based illness discriminating. Because of the well-defined nature of the illness and the simple accessibility of the cervix, numerous researchers have been able to do in vivo diagnostic studies on this organ. Several organizations have employed fiber-based Raman devices for diagnosis and compared their results to those obtained by colpos-copy. To produce a range of performance estimates, they have employed a variety of fiber probe designs and different multivariate statistical techniques, as indicated in **Table 1**. Huang and his co-worker established a simultaneous fingerprint and high-wave-number confocal Raman system for cervical pre-cancer diagnosis in 84 individual patients and proved the performance of this combination technique with a sensitivity of 81% and a specificity of 87% in other cervical cancer investigations. When utilizing multivariate diagnostic algorithms, Zeng and his co-worker investigated the feasibility of a label-free blood test based on blood plasma SERS on samples from 60 cervical cancer patients and found that it had a sensitivity and specificity of 96% and 92%, respectively. Other research has shown that Raman spectroscopy may be used to distinguish between responders and non-responders to radiotherapy in biopsies from patients with cervical cancer, as well as to detect high-risk human papilla-ma-virus strains in cervical cells. These findings, however, must be independently confirmed in a large research cohort. A table in a recent review paper on the use of Raman spectroscopy in the treatment of cervical cancer provides an outstanding overview of all relevant research. Beyond cancer detection, our team has shown that Raman spectroscopy may be used to follow biochemical changes in the cervix throughout pregnancy and gain a better knowledge of cervical remodeling during pregnancy and parturition.

5.2. Skin Cancer

The skin, being the largest organ in the in tegumentary system, serves as both the body's exterior barrier to the outside world and the tissue that is simplest to examine with light. The most prevalent malignancies in the world are melanocytic and non-melanocytic tumours, which have different biological origins. Skin cancers are among the simplest to investigate using optical methods since they are surface organ cancers; nevertheless, the complex, turbid structure of the skin makes it one of the most difficult clinical targets for optical diagnostics and monitoring. Early investigations utilized Raman spectroscopy to extract water concentration patterns in human skin, proving that in vivo Raman spectroscopy may be used for clinical monitoring. Since then, a large portion of skin Raman research has concentrated on developing Raman-based diagnostics. This research also led to the development of portable systems that are directly applicable to clinical practice, including equipment that can produce measurements in less than a second. As shown in **Table 1**, a number of organizations have made considerable expenditures in investigating skin cancers in order to enhance patient care. As a result, skin cancer studies have some of the highest recruitment of any Raman research published. Zeng and his co-worker used a Raman instrument to investigate 453 patients' melanocytic and non-melanocytic lesions, as well as malignant and premalignant mela-no-cytic lesions: cancer and pre-cancer versus benign lesions had a sensitivity of 90–99%, with a specificity of 15–54%. This research shows that Raman methods can be used to significantly minimize the need for superfluous biopsies, possibly by 50–100%. Other organizations have used multimodal methods to improve diagnostic performance, combining the strengths of Raman spectroscopy with fluorescence and diffuse reflectance techniques. Raman spectroscopy alone was shown to achieve 100 % sensitivity and specificity for distinguishing melanoma from benign pigmented lesions in one study of 76 patients, but only 72 % sensitivity and 64 % specificity for distinguishing non-melanoma skin cancers from pre-cancers and 68 % sensitivity and 55 % specificity for distinguishing non-melanoma cancers. When fluorescence and diffuse reflectance characteristics were added to the comparisons, the sensitivities/specificities increased to 100/100 %, 95/71 %, and 90/85 %, respectively. Irvine and his colleagues investigated 132 children with atopic dermatitis, combining natural moisturizing factor signals acquired by Raman scattering with genetic screening for filaggrin mutations, which are prevalent in atopic dermatitis. Raman signals had a sensitivity of 98.7% and a specificity of 86.8% in recognizing atopic dermatitis correlated with these mutations, according to the conclusions of this investigation. The use of a 488 nm based resonance technique to profile the consumption of fruits and vegetables in preschool-aged children has also been studied utilizing Raman spectral fingerprints of skin carotenoids. This investigation identified a connection between Raman signatures and parent-reported family engagement in nutritional education and -quality programs, revealing the Raman scattering's remarkable sensitivity to biochemical components.

5.3. Mouth Cancer

Mouth although endoscopy is not required, oral tissue is particularly easy to reach, alleviating the probe size restrictions for in vivo Raman studies. Oral cancer has been more common in the United States during the previous 40 years, and it is a global concern. In India, for example, it accounts for 10% of all malignancies. This cancer can spread quickly, emphasizing the importance of early identification and surveillance. Murali Krishna and his colleagues claim that they were able to distinguish between normal control, premalignant, and cancerous areas in 104 individuals, with prediction accuracies ranging from 72 to 96%. The same group evaluated the ability of Raman spectroscopy to identify cancer changes/cancer field effects in a cohort of 84 oral cancer and age-matched control patients in a more recent research. The accuracy of non-cancer regions in a smoking and non-smoking population was 75–98%, with the majority of misclassifications occurring between control locations in cancer patients and locations in smoking healthy controls. The sensitivity of Raman scattering to minor biochemical changes that may precede macroscopic illness is further demonstrated in this study. Another analysis revealed that normal oral tissue could be distinguished from three different lesion categories with per-class accuracies ranging from 82–89% in 199 patients, with 96% sensitivity and 99% specificities for normal versus malignant and 99% and 98% for normal versus potentially malignant, respectively. Given the significant need for oral cancer diagnosis, especially in low-resource settings, and the outstanding performance that Raman spectroscopy can accomplish in its detection, this field of study is ripe for clinical translation, but it will require a piece of low-cost equipment to be successful. The number of commercially accessible portable Raman devices has recently increased in the optical device industry; they are mostly used to identify pure compounds and trace elements. These devices, on the other hand, show that the technology exists for miniaturizing current clinical Raman systems, which might pave the way for the commercialization of Raman systems in low-resource situations.

5.4. Neurosurgery

In 2017, approximately 23,000 instances of brain and other nervous system cancers were estimated in the United States, with a 70% death rate. Brain and central nervous system cancers were the sixth most prevalent cause of death for those age between 15 to 39, according to the most current data (2010–2014) from the Central Brain

Tumor Registry of the United States (CBTRUS). Standard RS has been used in the bulk of studies on utilizing RS for brain tumour assessment. Standard RS has been used in the bulk of studies on utilizing RS for brain tumour assessment. Kast and his Co-worker used Raman peak intensities of 1004, 1300:1344, and 1660 $cm^{-1}$to produce pictures from frozen slices of brain tissue samples, which are indicative of protein and lipid content. With an in via Raman microscope (Renishaw) with an excitation wavelength of 785 nm, Raman spectra were obtained on five frozen section tissues (one normal, one necrotic, one GBM, and two infiltrating glioma). A 300-m2 step size was used to map the portions in their entirety. A 25-m step size was used to map smaller areas of interest, with each step corresponding to a distinct Raman spectrum. The pixels in each Raman picture were made up of data from the Raman characteristics that were chosen. The pixels in each Raman picture were made up of data from the Raman characteristics that were selected. A color was allocated to each peak (or peak ratio): red (1004 cm^{-1}), green (1300:1344 cm^{-1}), or blue (1660 cm^{-1}). The colored pictures allowed for the interpretation of brain matter, white matter, and diseased tissue barriers that paralleled the findings of neighboring hematoxylin and eosin-stained sections. Using the three Raman characteristics to perform leave-one-out discriminant function analysis yielded over 90% classification accuracy. A 785-nm laser (Innovative Photonic Solutions, NH, USA) and a high-resolution charge-coupled device spectroscopic detector were linked to the portable fiber optic probe (Em Vision LLC, FL, USA) (ANDOR Technology, Belfast, UK). For each measurement, the probe was put in direct contact with the brain at the resection cavity margin, with a 0.2-second acquisition period. To differentiate samples harboring invasive cancer cells from normal brain, researchers utilized a supervised machine learning boosted-trees classification method that took into account all spectral data.

6. Application of Raman Spectroscopy in Current Scenario

6.1. Raman Spectroscopy in Corona Virus Detection

During the sample preparation, concentrated viral particle stock of 7.05 × 107 TU/mL is to be diluted in 1:10 and 1:1000 ratio using two different diluents- sterile ultrapure water and human saliva to mimic the patient condition. Plain media in ultrapure water and saliva without viral particles are to be taken as negative controls. Besides, to check the specific biomolecule (DNA, RNA or proteins) which helps in the differentiation of viral particles, the samples were treated with either DNase or RNase or Proteinase K, respectively **[67]**. Dr Amit Dutta and his employees have used Raman spectra to identify the presence of RNA virions, generated using pLL 3.7 lentivirus vector system (based on HIV-I), with 7.05 x 107 TU/mL stock titre spiked in water and human saliva at 1:10 and 1:1000 dilutions. The infectivity of the viral particles was simultaneously confirmed by the observation of GFP expression in HEK293FT cells **(Figure 9)**. Reported spectral data from the saliva of individuals not known to have viral infection was used as a negative control. In this section of project work, a substitute Raman resolution was presented for the bias of current or past infection by SARS-CoV-2 from a really simply and safely collectable bio-fluid such as saliva. Raman spectroscopy can facilitation uncovering the molecular basis of disease like corona-virus and provide objective, quantifiable molecular information about their testing, diagnosis and treatment evaluation.

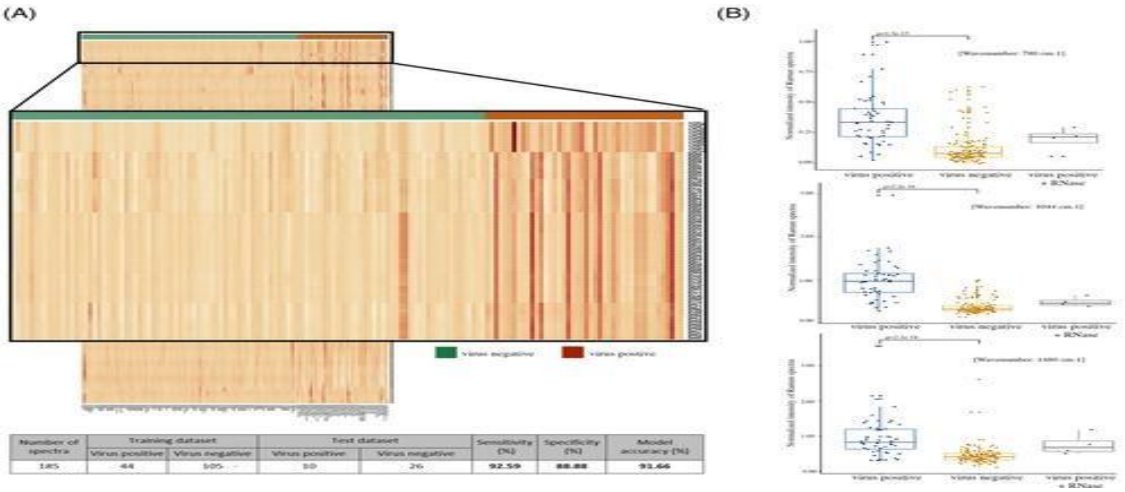

Fig. 9: *A Raman spectroscopy-based model to detect RNA viruses. A Heatmap representation of the 1200 features from the virus-positive and negative training sample set of Raman spectra with the zoomed-out version*

showing the peak intensities for the features selected (n = 65) for model construction. The table shows the overall sample statistics and summary of the performance of the 65-feature linear discriminant analysis-based model for the prediction of viral presence in the human saliva samples. B, Comparison of Raman spectra peaks between virus-positive, virus-negative and RNase-treated viral positive sample for RNA-specific constituents: the nitrogenous uracil base, ribose phosphate and A/G ring at 780, 1044 and 1480cm^{-1}, respectively by Wilcoxon rank-sum test.

Promiscuous experimental studies have been exhibited the faculty of Raman spectroscopy in tissue and RNA type virus characterization. Machine learning and artificial intelligence algorithms effectively promise of automating the recognizance and diagnosis of corona-virus.

By applying deep learning training with huge numbers of spectra, may also diagnosticate molecular arrangement among RNA-types virus, encouragement in RNA-type virus detection, and will play a prognosticator role in the aggressiveness of corona-virus. In enlargement to algorithm development, laser-tissue interactions that might result in tissue illness need to be examined to explicate the technology to clinical use. Raman scattering strength is proportional to the inverse of excitation wavelength to the fourth power and proportional to the intensity of the incident light. Even though more light explicates to more signal, the tissue has an illness threshold. The salivary Raman analysis was carried out following and slightly modifying the analytical protocol developed and validated by our group, leading to the observation of the whole biochemical pattern of saliva. The sample preparation procedure was compressed avoiding the filtration step, this way makes the analysis faster, inferior and more informative, modifying progressively the Raman procurement parameters. The procedure was intended for the free from harm collection of saliva, confine the sample handling and difficult or aggregate passages.

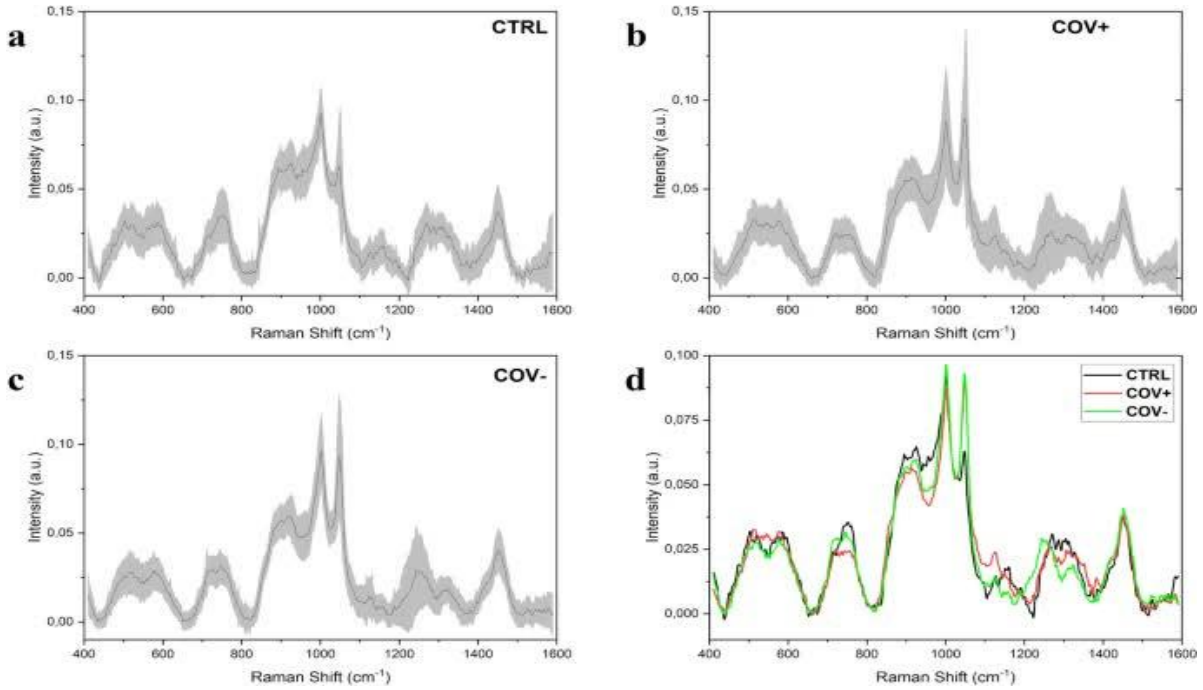

Fig.10: *Average Raman spectra obtained from (a) healthy subjects (CTRL), (b) patients affected by COVID19 (COV+) and (c) subjects with at least two negative SARS-CoV-2 tests after being positive (COV−). (d) Overlapped average spectra of the three experimental groups highlighting spectral differences. The grey bands represent the standard deviations.*

Figure 10 shows the salivary spectra obtained from the considered experimental groups, Healthy Subjects (CTRL) **Fig. 10a**, patients affected by COVID-19 (COV+) **Fig. 10b**, and subjects negative to the SARS-CoV-2 test with an ascertained episode of COVID-19 (COV−) **Fig. 10c**. The principal characteristics peaks and bands are located at 509, 577, 716, 748, 897, 922, 1000, 1048, 1126, 1155, 1249, 1288, 1317, 1384 and 1453 cm−1 highlighted in the overlapped spectrum **(Fig. 10d)**. The presented spectra are mainly dominated by the peaks attributed to C–N stretching and CH3 rocking in protein backbone (897 and 1155 cm−1) and by the signal at 1453 cm−1 assigned to the C–H stretching of glycol-proteins, mostly generated from mucinous. Crucial importance in the signal discrimination between the different experimental groups can be attributed to the peaks located at 748, 922, 1048, 1249 and 1126 cm−1, which present significant differences from a preliminary visual

spectral investigation **(Fig. 10d)**. Te peak positioned at 748 cm−1 is mainly related to the O–O stretching in oxygenated proteins and glycoproteins including mucinous and proline-rich glycoprotein and to the symmetric breathing of tryptophan (Trp), while the peak at 922 cm−1 is related to simple and branched carbohydrates including glucose and glycogen. Probably, the peaks of greatest interest are located at 1048 and 1126 cm−1 that can be respectively attributed to the Trp and phenylalanine signal and to the C–N and C–C stretching. The potential assignment of other peaks and bands are listed in Table-2:

Table-2: *Attribution of the most legendary signals revealed from the Raman salivary analysis (±10 cm−1), Trp, Cys, Phephenylalanine.*

S.No.	Position of the Raman peak(cm^{-1})	Attribution
1	512	Phosphorylated protein and lipids
2	580	Trp, Cys
3	720	Phospholipids
4	750	O–O stretching, symmetric breathing of Trp
5	899	Mono and disaccharides C–O–C skeletal modes
6	925	Glucose/glycogen
7	1000	Phe ring modes
8	1050	C–N and C–C protein stretching
9	1130	Trp, Phe
10	1155	Glycogen
11	1250	Secondary bands of amide III
12	1290	Phosphodiester groups in nucleic acids
13	1320	Amide III (α-helix structures)
14	1385	C–H rocking in lipids
15	1455	General fatty acids, C–H stretching of glycoproteins

The principal differences between the evaluate groups in terms of intensities are pointed out by the subtraction spectra accomplish between the averages Raman signals obtained **(Fig. 11)**. The highest differences can be detected in the comparison between the CTRL group with the CoV-positive and CoV-negative groups **(Fig. 11 a, b)**. All the differences in intensities (ΔI) were considered for ±0.005 ΔI, identifying peaks at 748, 897, 922, 1048, 1126, 1249, 1317 and 1348 cm^{-1}. Interestingly, peaks at 1048 and 1126 cm^{-1} govern the subtraction spectra, with substantial differences between the CTRL experimental group and the CoV-positive and CoV-negative respectively **(Fig. 11 a, b)**. The strong signal in correspondence of these two regions is normally associated with an environment rich in aromatic amino acids, in particular tryptophan and phenylalanine (1048 cm^{-1}, **Table-2)**. Interestingly, the two identical peaks were also recognized as character bsignals from viruses of the corona-virus family, probably being confluent in the viral protein structure or with the interactions with physiologically expressed molecules. Recent studies conducted on SARS-CoV-2 and on other types of corona-viruses display the important presence of aromatic amino acids, including Trp, in the virus spike glycoproteins, label the so-called Trp-rich regions confluent in the interaction between the virus and the receptor Angiotensin-Converting Enzyme type-2 (ACE2). In terms of Raman signal, an abundance of aromatic amino acids and saccharides in saliva could exhort the different intensities evident in the relative regions for CoV- positive and CoV-negative experimental groups **(Fig. 11 a, b)**. The presence in CoV-positive saliva of potential viral particles in huge amount can be easily analysed by the high viral title reached during the COVID-19 infection with the oral cavity as one of the first infection sites, together with the upper and lower respiratory tracts due to the high expression of ACE2 receptor. Moreover, the assignment of the main differences to protein species and correction could be made clear also with the expression of different molecules of the immune response in the first and late stages of the infection. The complex and specific manifestation pattern of immunity proteins, such as IgA, IgM and IgG, can last up to 3 months leading to the detectable signals both in serum and in saliva. Specifically, the saliva represents a reliable biofluid for the detection being involved in the first phases of infection with the tenacious presence of biological molecules precisely involved in the SARS-CoV-2 presence. Clinical data collected from CoV-negative patients revealed periods of negativization between 8 and 90 days explaining the persistence in the Raman signals of differences when compared with CTRL and CoV-positive **(Fig. 11 b, c)**.

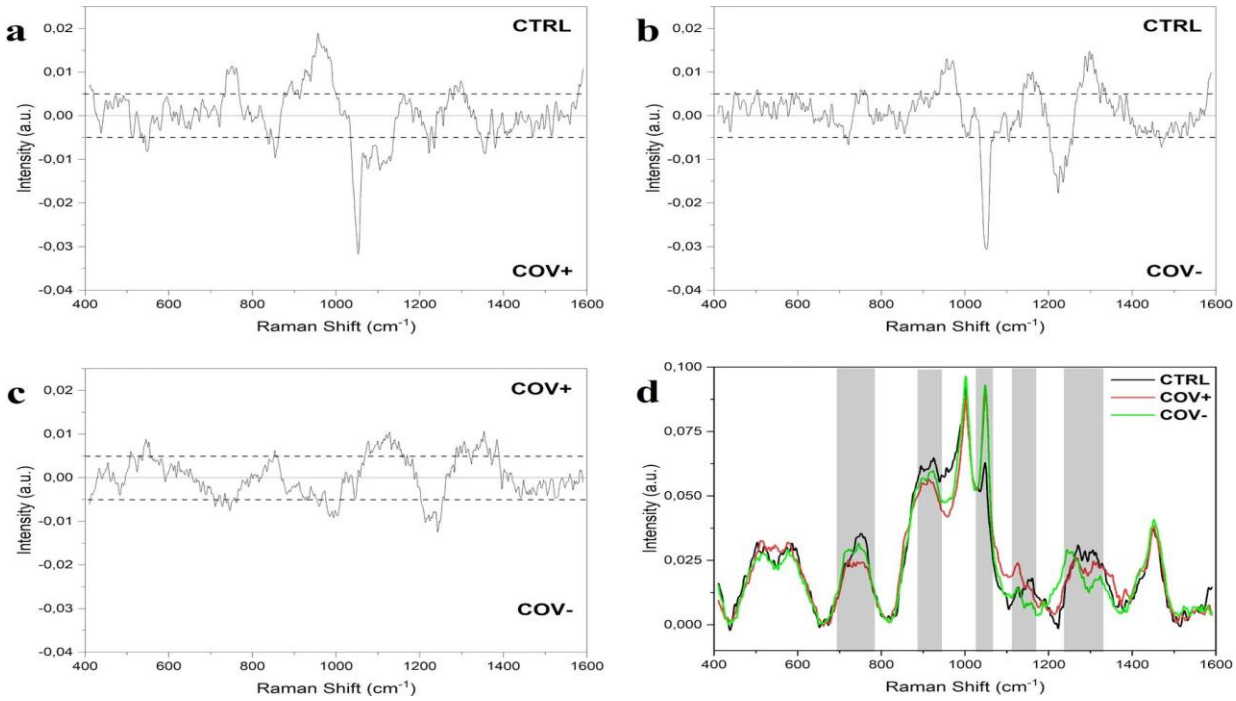

Fig.11: *Subtraction Raman spectra of (a) the average CTRL signal versus the average signal of CoV-positive , (b) the average CTRL signal versus the average CoV-negative spectrum and c) the average CoV-positive signal versus the average CoV−negative signal. The ± 0.005 ΔI interval is indicated in the graphs, confirmed by the error propagation from the spectra standard deviation. d) Overlapped average spectra of CTRL, CoV-positive and CoV-negative with the main different region highlighted.*

These results are confirmed by the fewer characterised differences in terms of peak intensities in the subtraction spectrum of CoV-positive and CoV-negative concerning the peaks at 1048 and 1126 cm^{-1} **(Fig. 11c)**. In this case, it is possible to observe a discontinuous trend of the subtraction spectrum, with bands belonging to lipids (509 cm^{-1}), carbohydrates (922 and 1155 cm^{-1}) and structured proteins (1317 cm^{-1}) tending to the CoV-positive groups with respect to the CoV-negative. With the information obtained from the subtraction spectra, it is desirable to identify four regions of particular interest in the spectra obtained from CTRL, CoV-positive and CoV-negative groups **(Fig. 11d)**, where the trends of the curves are modified by differences in intensities and in presence of specific peaks. Preprocessing the raw data helps eliminate unwanted signals enhance Raman spectral features and allow more reproducible data for qualitative and quantitative analysis.

6.2. Raman Spectroscopy in Characterization of Nano-Particles

In this section of the project report we will discuss how Raman Spectroscopy characterized nano-particle will the help of surface enhancement Raman Spectroscopy. Now do this for Gold and Silver nano-particles. Now demonstrate how SERS enhancement is contingent on interactions between the target molecule and the SERS substrate. As a consequence, the primary challenge for a successful SERS enhancing technique is the preparation of the SERS substrate. The preponderance of the SERS enhancement is due to EM enhancement, which is highly dependent on the size, shape, and structure of the material used to build the substrate. SERS substrates are often constructed using nano-structured plasmonic materials including such gold (Au), silver (Ag), and copper (Cu). Cu, on the other extreme, has a constrained application due to oxidation difficulties in air. Gold and silver, on the other side, are the most widely used due to their higher stability over copper and, more significantly, their LSPR frequencies in the visible to near-infrared spectrum, where most Raman scattering occurs. In this section, we will explore the use of these plasmonic noble metals as SERS substrates. Gold and silver nanoparticles have unique optical characteristics that make them extremely useful for nanoscience and nanotechnology applications. Gold nanoparticles, in particular, have numerous applications in regular activities, and they have been widely utilized to develop various nanostructured assemblies due to their processability, simple surface functionalization, chemical stability, and biocompatibility**.** Silver nanoparticles, on the other hand, have grown in popularity in biomedicine due to their antibacterial action against a variety of bacteria, fungi, protozoa, and viruses. Although gold and silver nanoparticles have strong plasmon absorption bands that may be modulated in the visible spectral range, they have become one of the most widely utilised materials in plasmonics, ultrasensitive detection, and surface-enhanced Raman spectroscopy. Since gold and silver nanoparticles have strong plasmon absorption bands that may be modulated in the visible spectral range,

they have become one of the most widely utilised materials in plasmonics, ultrasensitive detection, and surface-enhanced Raman spectroscopy (SERS). Because of their LSPR characteristics, nano-particles of noble metals are the most extensively employed materials for the preparation of SERS substrates. These characteristics are only significant when the materials are nanoscale, i.e. shorter than 100 nm in dimension. Several publications on the synthesis and development of noble metal nanostructures with customizable forms and sizes for SERS applications are presently available. Colloidal mono-disperse metal nano-particles exhibit significant SERS enhancement due to the nano-particles' predetermined size and shape. A comprehensive investigation of colloidal Ag nanostructures with diameters ranging from 60 to 100 nm confirmed that the SERS enhancement was dependent on the shape and size of the nano-particles.

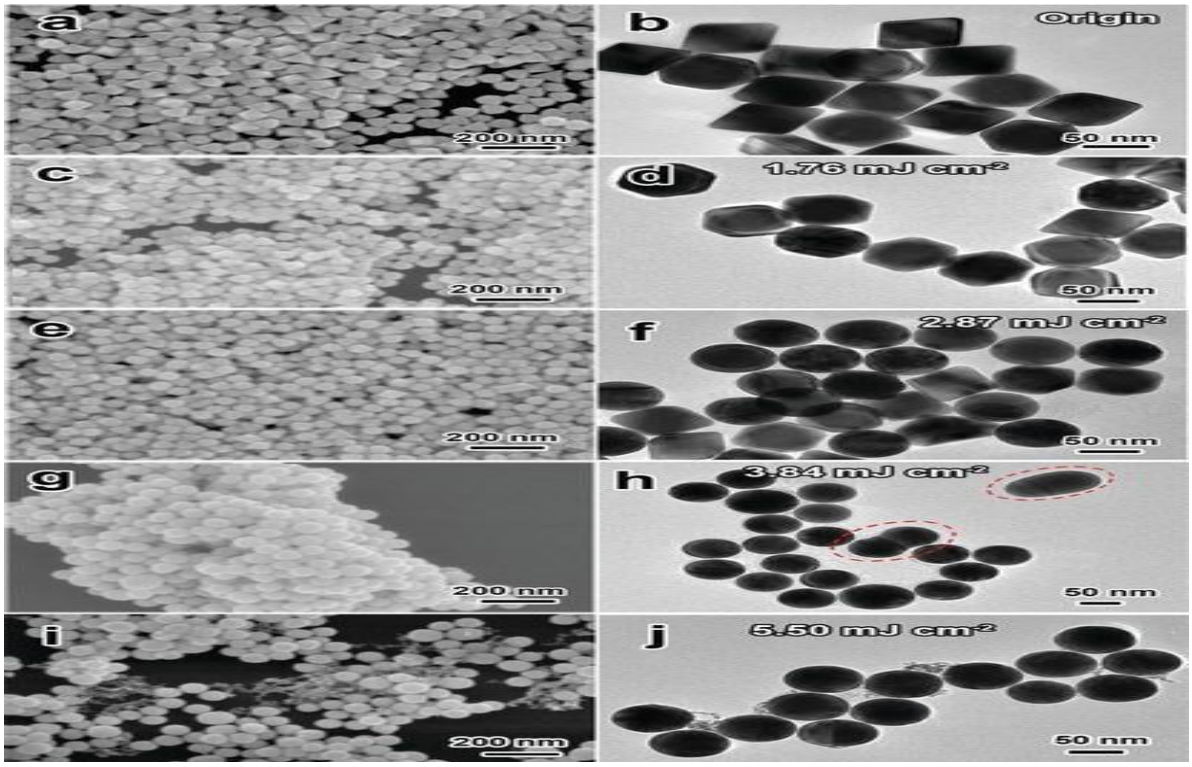

Fig. 12: *SEM and TEM micrographs of laser irradiated various shaped colloidal SERS Au nanoparticles. Au nanoparticles were prepared by a polyol route at 195 C. (a, b) original octahedral nanoparticles and nanoparticles in (c, d), (e, f), (g, h) and (i, j) were irradiated with a Nd: YAG laser (532 nm, pulse duration:10 s) operated at 20 Hz with laser fluences equal to 1.76, 2.87, 3.84 and 5.50 mJ.cm^{-2} respectively.*

It was discovered that EFSERS improves with increasing nano-particle size from 60 to 100 nm, with cubical nano-particles with sharp edges producing EFSERS on the order of 10^5 when compared to almost spherical Ag nano-particle EFSERS (in the order of10^4). The shape dependency of the E is mostly attributable to the concentrated nonuniform electric field density (hot spots) along the sharp edges of the cubical Ag nanoparticle, whereas the field spread uniformly over the entire surface of the spherical nanoparticles. It has been demonstrated, for example, that the strength of the hot spots may be modified by changing the shape of the colloidal nanoparticles from spherical to anisotropic. It was observed that a spherical nanoparticle has a weak hot spot when compared to an anisotropic particle, resulting in an increase in EFSERS from 10^4 to 10^7, making anisotropic particles acceptable for single molecule detection. The researchers also demonstrated that increasing the anisotropy or aspect ratio of such colloidal metal nano-particles can enhance the EFSERS.

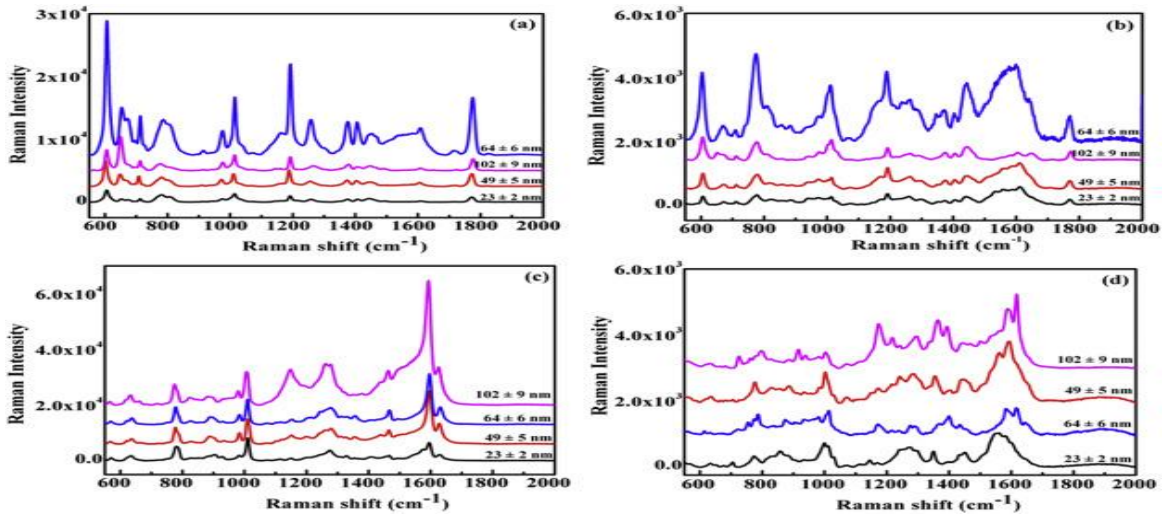

Fig. 13: *Surface-enhanced Raman spectroscopy coupled with Gold nano-particles.*

Using aggregated colloidal Ag nano-clusters, an amplification factor of up to 10^4 was also observed. Many researchers are interested in the SERS application of colloidal gold (Au) nano-particles. Gold is more expensive than Ag, and gold ultimately resulted in moderate EFSERS to Ag nano-particles. Gold, on the other hand, has excellent biocompatibility characteristics, making it an effective SERS candidate for biological secimen. Quester and his colleagues investigated the SERS characteristics of Au nanoparticles of various sizes (10–200 nm) and shapes (spherical, triangles, hexagons, and pentagons). Similarly, Liu et al. proposed a laser irradiation rapid synthesis method for different shaped colloidal gold nanoparticles for SERS applications (**Fig. 13**). They have effectively demonstrated detection of Rhodamine 6G (R6G) dyes at concentration levels as low as 10^{-11} M using nanospheres of Au nano-particles.

6.2.1. Properties of Gold Nano-particles

The gold nano-particles properties are the wine-red solution. The interactions of gold nanoparticles play an important role in their properties. There are different sizes of gold nanoparticles start from 1 nm to 8 μM, and various shapes; for example, spherical ring, suboctahedral, icosahedral tetrahedral, decahedral, octahedral, and nano-rods. Gold nanoparticles have been commonly utilized in the radiation medicine field as a radiant enhancer and improvement in the therapy of radiation because the ability in drug delivery. Furthermore, Au/NPs have different uses or applications in nanotechnology as a platform for labeling of proteins and biomolecular detection. The Au/NPs are non-toxic particles with large surface area and can be modified with other molecules, and used in biomedical fields. The significance of Au/NPs in biochemistry field is due to the compatibility, and optical properties.

Table-3: *Optical Property of Gold Particle of Varying Radius***.**

S.No	Radius(nm)	Extinction Efficiency	Resonance Wavelength (nm)	Lower Half PeakWavelength (nm)	Upper Half Peak Wavelength (nm)	Half Peak Width (nm)
1	**2**	**0.261**	**522**	**504**	**538**	34
2	**3**	**0.392**	**522**	**504**	**538**	34
3	**5**	**0.658**	**522**	**504**	**538**	34
4	**6**	**0.794**	**522**	**504**	**539**	35
5	**7**	**0.933**	**523**	**504**	**539**	35
6	**8**	**1.07**	**523**	**504**	**539**	35
7	**10**	**1.37**	**523**	**505**	**540**	35
8	**15**	**2.16**	**525**	**506**	**541**	35
9	**20**	**3.07**	**526**	**508**	**545**	37
10	**25**	**4.06**	**529**	**510**	**550**	40
11	**30**	**5.05**	**534**	**513**	**557**	44
12	**35**	**5.89**	**540**	**517**	**567**	50
13	**40**	**6.5**	**549**	**520**	**578**	58

Nanoparticles are good therapeutic agents due to their ease transport in the diseased cell and carrier-loading drug. Gold nanorods are widely used in the vivo cell imaging because of resonance absorption plasmon and scatter of light in IR. In addition, colloidal Au/NPs have the very small size to introduce in the tissues and cells of biological molecules such as proteins and DNA. Because of their electronic properties, Au/NPs have been commonly utilized in analytical methods and used as an electrode sensor of different samples.

7. Conclusion

Raman spectroscopy is a variety of vibrational spectroscopy that requires a thorough understanding of light's characteristics. It provides a chemical "fingerprint" of the substance examined and is thus commonly employed when identifying unknown materials. Raman spectroscopy is a very effective technique in a variety of disciplines, including biomedical, material science, pharmaceutical nano-science, and sensor applications. With the emergence of nanotechnology as an enabling technology, applications of noble metal nanostructures with remarkable opto-electrical properties for SERS applications have emerged as a major area of R&D, which includes not only the synthesis of plasmonic nanostructures for SERS substrates, but also nano-scale patterning of surfaces to enhance the effect. Producing highly sensitive, large area resilient, and reusable SERS substrates using low-cost fabrication techniques presents a challenge. Raman spectroscopy can serve in the discovery of disease's molecular foundation and offer objective, quantitative molecular information for diagnosis and treatment evaluation. Numerous experimental studies have demonstrated Raman spectroscopy's capability for tissue characterisation. The development of comprehensive spectrum databases and tissue categorization techniques that can be compared to current gold standards is essential for clinical application. Best-practice data processing, acquisition, and categorization techniques must be established and implemented. Various interferents, such as fluorescence, a process that generally competes with Raman scattering, might make it very difficult to understand Raman spectra of biological samples. Preprocessing raw data eliminates unnecessary signals, enhances Raman spectral characteristics, and enables for more repeatable data for qualitative and quantitative analysis. However, we and others show that the average preprocessing technique employed can have a significant impact on tissue categorization results. In addition to providing best-practice frequency band preprocessing approaches, consideration must be used when developing classification algorithms for diagnostic assessment. To confirm that algorithms developed on ex vivo specimens are applicable to in vivo tissues, validation studies must be performed successfully. Machine learning algorithms provide the potential of automating cancer detection and diagnosis. Deep learning training with such a large number of spectra may also identify molecular patterns among cancer species, aid with margin detection, and become indicators of cancer aggressiveness. The continuing development of Raman spectrum databases, tissue categorization techniques, and instrument designs aimed at obtaining data with higher resolution, shorter collection periods, and higher accuracy will ensure that Raman spectroscopy becomes a valuable clinical tool.

8. Reference

[1]. Abdelsalam Mohammed; Theoretical Studies of Raman Scattering; Printed by Universitetsservice: US-AB; 2011; page (14).
[2]. H. J. Hibben; The Raman Effect and Its Chemical Applications; Reinhold Publishing Company; 1939.
[3]. D. A. Long; The Raman Effect; John Wiley & Sons Ltd.; West Sussex; 2002.
[4]. Pushkar P. Kalantari, Rakesh R. Somani and Dinesh T. Makhija; Raman spectroscopy: A potential technique in analysis of pharmaceuticals; Pelagia Research Library; 2010; page (1).
[5]. Gregory W. Auner, S. Kiran Koya, Changhe Huang, Brandy Broadbent, Micaela Trexler, Zachary Auner, Angela Elias, Katlyn Curtin Mehne & Michelle A. Brusatori; Applications of Raman spectroscopy in cancer diagnosis; Cancer Metastasis Rev.; 2018; page 691–717.
[6]. AZOMaterials;https://d12oja0ew7x0i8.cloudfront.net/images/Article_Images/ImageForArticle_15797(1).jpg
[7]. Raj Kumar; Atomic and Molecular spectra: Laser; Kedhar Nath Ram Nath Publication Meerut Delhi; 2008; Page (336-348).
[8]. Coleman Krawczyk; The Raman Effect.
[9]. P. F. Bernath; Light scattering and the Raman effect; Oxford University Press Inc; 2005; 2nd ed.; page(293–317).
[10]. J. R. Ferraro, K. Nakamoto & C. W. Brown; Introductory Raman spectroscopy San Diego: Academic; 2003; 2nd ed.
[11]. Slobodan Sasic; Pharmaceuticals applications of Raman Spectroscopy; Wiley; 2008.
[12]. D.C. Harris Och & M.D. Bertolucci; Symmetry and Spectroscopy; Oxford University Press; 1978.
[13]. J.M. Chalmers & P.R. Griffiths; Handbook of Vibrational Spectroscopy; Wiley; 2002.
[14]. L.A.Wooduard; Introduction to theory of Molecular vibrations and vibrational spectroscopy; Clarendon Press; 1972.
[15]. P.W. Alkins; Molecular Quantum Mechanics; Oxford University Press; 1983.
[16]. Barbara A. Schreiber; Schrödinger equation: Matter and Energy; Encyclopedia Britannica; 2021; https://www.britannica.com/science/Schrodinger-equation.
[17]. Fujitsu; Supercomputer Achieves World Record in Computational Quantum Chemistry; PHYSORG; 2010; https://phys.org/news/2010-05-fujitsu-supercomputer-world-quantum-chemistry.html.
[18]. J. M. Hollas; Modern spectroscopy; New York: Wiley; 2004; 4th ed..
[19]. H. Abramczyk; Introduction to laser spectroscopy; New York: Elsevier Science Ltd.; 2005.
[20]. Eric Heller; The Semiclassical Way to Dynamics and Spectroscopy: Born-Oppenheimer Approximation and Its Implications (Chapter 16); Princeton University Press; 2018; https://doi.org/10.23943/9781400890293-019.

[21]. David M. Hanson, Erica Harvey, Robert Sweeney and Theresa Julia Zielinski; The Born-Oppenheimer Approximation; Chemical Education Digital Library; 2020. https://chem.libretexts.org/Bookshelves/Physical_and_Theoretical_Chemistry_Textbook_Maps/Book%3A_Quantum_States_of_Atoms_and_Molecules_(Zielinksi_et_al)/10%3A_Theories_of_Electronic_Molecular_Structure/10.01%3A_The_Born-Oppenheimer_Approximation.

[22]. P. W. Atkins; Molecular Quantum Mechanics; Oxford University Press; 2001.

[23]. Szabo and S. N. Ostlund; Modern Quantum Chemistry; McGraw–Hill; 1989; page(43-45);https://books.google.co.in/books?hl=en&lr=&id=KQ3DAgAAQBAJ&oi=fnd&pg=PP1&dq=A.+Szabo+and+S.+N.+Ostlund.+Modern+Quantum+Chemistry.+McGraw%E2%80%93Hill,+New+York,+1989.&ots=P_qHKWvkdL&sig=m4QdwvQeUnlfTTnvhSUDBI1qAuE#v=onepage&q&f=true.

[24]. Prof. Thomas Pruschke; Introduction to solid state theory; Gottingen WiSe; 2013; https://www.tifr.res.in/~kbmaiti/Course/Note1_Thomas.pdf.

[25]. Pauli Exclusion Principle; Wikipedia, the free encyclopedia; https://en.wikipedia.org/wiki/Pauli_exclusion_principle.

[26]. Slater determinant; Wikipedia; the free encyclopedia; https://en.wikipedia.org/wiki/Slater_determinant.

[27]. Xin Zhang, Kui Xiao, Chaofang Dong, Junsheng Wu, Xiaogang Li & Yizhong Huang; In situ Raman spectroscopy study of corrosion products on the surface of carbon steel in solution containing Cl− and SO42-; Engineering Failure Analysis; 2011; http://dx.doi.org/10.1016%2Fj.engfailanal.2011.03.007.

[28]. J.R. Ferraro; Introductory Raman spectroscopy; Academic press; 2003.

[29]. Paul Rostron, Safa Gaber and Dina Gaber ; Raman Spectroscopy: A Review; International Journal of Engineering and Technical Research (IJETR); 2016.

[30]. Margaret Smith, Karen Thompson and Frances Lennard; A literature review of analytical techniques for materials characterization of painted textiles—Part 2: spectroscopic and chromatographic analytical instrumentation; Journal of the Institute of Conservation; 2017; https://doi.org/10.1080/19455224.2017.1365739.

[31]. Raj Kumar; Atomic And Molecular Spectra: Laser; Sangam Publication; 2012; Volume-38,Page (336).

[32]. JR Ferraro, K Nakamoto, CW Brown; Introductory Raman Spectroscopy; (2nd ed.); Amsterdam: Academic Press; 2003; Page (434).

[33]. Eric Olaf Potma and Shaul Mukamel; Coherent Raman Scattering Microscopy: Theory of Coherent Raman Scattering; CRC Press/Taylor & Francis Group; 2013; https://mukamel.ps.uci.edu/publications/pdfs/727.pdf.

[34]. P.D. Maker, and R.W. Terhune, Study of optical effects due to an induced polarization third order in the electric field strength, Phys. Rev.; 1966.

[35]. Coherent Anti-Stokes Raman Scattering Microspectrometer; Technology and Applications Center Newport Corporation; https://www.newport.com/medias/sys_master/images/images/hc0/h9a/8797076226078/Coherent-Anti-Stokes-Raman-Scattering-App-Note-36.pdf.

[36]. Bruce Hudson, William Hetherington, Stephen Cramer, Ilan Chabayt, and Gary K. Klauminzerf; Resonance enhanced coherent anti-Stokes Raman scattering; Proceedings of the National Academy of Sciences of the United States of America; 1976; https://www.pnas.org/content/pnas/73/11/3798.full.pdf.

[37]. B. Sharma, R. R Frontiera, A. I. Henry, E. Ringe and R. P. Van Duyne; SERS: Materials, applications, and the future. Materials today; 2012.

[38]. G. C. Schatz; Electrodynamics of nonspherical noble metal nanoparticles and nanoparticle aggregates; Journal of Molecular Structure: THEOCHEM; 2001.

[39]. P. L. Stiles, J. A. Dieringer, N.C. Shah, and R.P. Van Duyne; Surface-enhanced Raman spectroscopy; Annual Review of Analytical Chemistry; 2008.

[40]. C. L. Haynes, C.R. Yonzon, X. Zhang and R. P. Van Duyne; Surface-enhanced Raman sensors:early history and the development of sensors for quantitative biowarfare agent and glucose detection; Journal of Raman Spectroscopy; 2005.

[41]. Eric Le Ru and Pablo Etchegoin; Principles of Surface-Enhanced Raman Spectroscopy and Related Plasmonic Effects; Elsevier: London; 2009.

[42]. D. Zeisel, V. Deckert, R. Zenobi and T. Vo-Dinh; Near-field surface-enhanced Raman spectroscopy of dye molecules adsorbed on silver island films; Chemistry Physics Letter; 1998.

[43]. Kudelski; Analytical applications of Raman spectroscopy; Talanta; 2008.

[44]. S. Schlücker; Surface-enhanced Raman spectroscopy: Concepts and chemical applications; Angewandte Chemie International Edition ; 2014.

[45]. Fourier-transform spectroscopy; Wikipedia: the free encyclopedia; https://en.wikipedia.org/wiki/Fourier-transform_spectroscopy.

[46]. Fani Madzharova, Zsuzsanna Heiner and Janina Kneipp; Surface-enhanced hyper Raman scattering (SEHRS) and its applications; Chemical Society Reviews; 2017.

[47]. N. L. Gruenke, M. F. Cardinal, M. O. McAnally, R. R. Frontiera, G. C. Schatz and R. P. Van Duyne; Ultrafast and nonlinear surface-enhanced Raman spectroscopy; Chemical Society Reviews; 2016.

[48]. K. Kneipp, Y. Wang, H. Kneipp, L.T. Perelman, I. Itzkan, R. R. Dasari and M. S. Feld; Single molecule detection using surface-enhanced Raman scattering (SERS); Physical review letters;1997.

[49]. Wu-Hu Li, Xiao-Yuan Li and Nai-Teng Yu; Surface-enhanced hyper-Raman scattering and surface-enhanced Raman scattering studies of electroreduction of phenazine on silver electrode; Chemical Physics Letters; 2000.

[50]. C. B. Milojevich, B. K. Mandrell, H. K. Turley, V. Iberi, M. D. Best and J. P. Camden; Surface-enhanced hyper-Raman scattering from single molecules; The Journal of Physical Chemistry Letters; 2013.

[51]. H. K. Turley and J. P. Camden; A nonlinear approach to surface-enhanced sensing in the short-wave infrared; Chemical Communications; 2014.

[52]. Nebu John and Sony George; Spectroscopic Methods for Nano-materials Characterization; Elsevier; 2017; https://ars.els-cdn.com/content/image/3-s2.0-B9780323461405000054-f05-13-9780323461405.jpg.

[53]. Lindsey A Torre, Freddie Bray, Rebecca L Siegel, Jacques Ferlay, Joannie Lortet-Tieulent and Ahmedin Jemal; Global cancer statistics 2012; A Cancer Journal for Clinicians: NCBI Literature Resources; 2015 Feb; https://doi.org/10.3322/caac.21262.

[54]. Elizabeth M Kanter, Elizabeth Vargis, Shovan Majumder, Matthew D Keller, Emily Woeste, Gautam G Rao and Anita Mahadevan-Jansen; Application of Raman spectroscopy for cervical dysplasia diagnosis; Journal of Biophotonics; 2009 Feb; https://doi.org/10.1002/jbio.200910001.

[55]. Elizabeth M. KANTER, Shovan MAJUMDER, Gary J. KANTER, Emily M. WOESTE, and Anita MAHADEVAN-JANSEN; Effect of hormonal variation on Raman spectra for cervical disease detection; American Journal of Obstetrics and Gynecology: NCBI Literature Resources; 2009 May; https://dx.doi.org/10.1016%2Fj.ajog.2008.11.024.

[56]. Shiyamala Duraipandian, Wei Zheng, Joseph Ng, Jeffrey J H Low, Arunachalam Ilancheran and Zhiwei Huang; Near-infrared-excited confocal Raman spectroscopy advances in vivo diagnosis of cervical precancer; Journal of biomedical optics: NCBI Literature Resources; June 2013; https://doi.org/10.1117/1.jbo.18.6.067007.

[57]. M S Vidyasagar, K Maheedhar, B M Vadhiraja, Donald J Fernendes, V B Kartha nad C Murali Krishna; Prediction of radiotherapy response in cervix cancer by Raman spectroscopy: a pilot study; Biopolymers: NCBI Literature Resources; 2008 June https://doi.org/10.1002/bip.20923.

[58]. Elizabeth Vargis, Yi-Wei Tang, Dineo Khabele, and Anita Mahadevan-Jansen; Near-infrared Raman Microspectroscopy Detects High-risk Human Papillomaviruses; Translational Oncology- Journal: Elsevier; 2012 June; https://doi.org/10.1593/tlo.12106.

[59]. Christine M O'Brien, Elizabeth Vargis, Bibhash C Paria, Kelly A Bennett and Anita Mahadevan-Jansen, Jeff Reese; Raman spectroscopy provides a noninvasive approach for determining biochemical composition of the pregnant cervix in vivo; Acta Paediatrica: NCBI Literature Resources; 2014 July; https://doi.org/10.1111/apa.12630.

[60]. Zhiwei Huang, Seng Khoon Teh, Wei Zheng, Jianhua Mo, Kan Lin, Xiaozhuo Shao, Khek Yu Ho, Ming Teh and Khay Guan Yeoh; Integrated Raman spectroscopy and trimodal wide-field imaging techniques for real-time in vivo tissue Raman measurements at endoscopy; Optics Latter: NCBI Literature Resources; 2009 March; https://doi.org/10.1364/ol.34.000758.

[61]. Jianhua Zhao, Harvey Lui, David I McLean and Haishan Zeng; Real-time Raman spectroscopy for non-invasive skin cancer detection - preliminary results; Annual International Conference of the IEEE Engineering in Medicine and Biology; 2008; https://doi.org/10.1109/iembs.2008.4649861.

[62]. Gráinne M O'Regan, Patrick M J H Kemperman, Aileen Sandilands, Huijia Chen, Linda E Campbell, Karin Kroboth, Rosemarie Watson, Marion Rowland, Gerwin J Puppels, W H Irwin McLean, Peter J Caspers and Alan D Irvine; Raman profiles of the stratum corneum define 3 filaggrin genotype-determined atopic dermatitis endophenotypes; Journal of allergy and clinical immunology: NCBI Literature Resources; 2010 Sept.; https://doi.org/10.1016/j.jaci.2010.04.038.

[63]. S P Singh, Atul Deshmukh, Pankaj Chaturvedi and C Murali Krishna; In vivo Raman spectroscopic identification of premalignant lesions in oral buccal mucosa; Journal of biomedical optics: NCBI Literature Resources; 2012 October; https://doi.org/10.1117/1.jbo.17.10.105002.

[64]. Rebecca L. Siegel, Kimberly D. Miller and Ahmedin Jemal; Cancer statistics-2017; A Cancer Journal for Clinicians: NCBI Literature Resources; 2017 January; https://doi.org/10.3322/caac.21387.

[65]. Quinn T Ostrom, Haley Gittleman, Peter Liao, Toni Vecchione-Koval, Yingli Wolinsky, Carol Kruchko and Jill S Barnholtz-Sloan; CBTRUS Statistical Report: Primary brain and other central nervous system tumors diagnosed in the United States in 2010–2014; Neuro-oncology: oxford Academic; 2017 October; https://doi.org/10.1093/neuonc/nox158.

[66]. Gregory W. Auner S. Kiran Koya, Changhe Huang, Brandy Broadbent, Micaela Trexler, Zachary Auner, Angela Elias, Katlyn Curtin Mehne and Michelle A. Brusatori; Applications of Raman spectroscopy in cancer diagnosis; Cancer and Metastasis Reviews; 2018 December; https://doi.org/10.1007/s10555-018-9770-9.

[67]. Vikram Singh And Vasavi Dathar; Surface Enhancement Raman Spectroscopy In Covid-19 Testing; International Journal Of Advanced Research; 2021 July.

[68]. Gunjan Tyagi, A.D., Raviraj Deshpande, Vikram Gota & Murali Krishna Chilakapati; Saliva Raman Spectroscopy: Explorations of Sampling Methods; In 18th European Conference on the Spectroscopy of Biological Molecules.2019; Dublin, Ireland: ECSBM18.

[69]. Sanket Desai, Saket V. Mishra, Asim Joshi, Debashmita Sarkar, Arti Hole, Rohit Mishra, Shilpee Dutt, Murali K. Chilakapati, Sudeep Gupta and Amit Dutt; Raman spectroscopy-based detection of RNA viruses in saliva: A preliminary report; Journal of Biophotonic; 2020 July.

[70]. S. Nie and SR . Emory; Probing single molecules and single nanoparticles by surface-enhanced Raman scattering; Science; 1997.

[71]. C. Carlomagno, P. I. Banf, A.Gualerzi, S. Picciolini, E.Volpato, M. Meloni , A. Lax, E. Colombo, N.Ticozzi, F.Verde3, V. Silani and M. Bedoni; Human salivary Raman fngerprint as biomarker for the diagnosis of amyotrophic lateral sclerosis; Scientific Reports; 2020; https://doi.org/10.1038/s41598-020-67138-8.

[72]. Virkler, K. & Lednev, I. K.; Forensic body fluid identification: The Raman spectroscopic signature of saliva; Analyst; 2010 March.

[73]. S. Gonchukov, A. Sukhinina, D. Bakhmutov, & S. Minaeva; Raman spectroscopy of saliva as a perspective method for periodontitis diagnostics; Laser Physics Letter; 2011 November.

[74]. Ewelina Wiercigroch, Ewelina Szafraniec, Krzysztof Czamara, Marta Z Pacia, Katarzyna Majzner, Kamila Kochan, Agnieszka Kaczor, Malgorzata Baranska & Kamilla Malek; Raman and infrared spectroscopy of carbohydrates: A review; Spectrochimica Acta Part A Molecular and Biomolecular Spectroscopy; 2017 May.

[75]. Dieter Naumann; FT-Infrared and FT-Raman spectroscopy in biomedical research; Appllied: Spectroscopy Review; 2001 October; https://doi.org/10.1081/ASR-100106157.

[76]. Rygula, K. Majzner, K. M. Marzec, A. Kaczor, M. Pilarczyk & M. Baranska; Raman spectroscopy of proteins: A review; Journal of Raman Spectroscopy; 2013 July; https://doi.org/10.1002/jrs.43355.

[77]. Cui Fan, Zhiqiang Hu, Lela K Riley, Gregory A Purdy, Azlin Mustapha & Mengshi Lin; Detecting food and waterborne viruses by surface-enhanced Raman spectroscopy; Journal of Food Science; 2010 July; https://doi.org/10.1111/j.1750-3841.2010.01619.xx.

[78]. Yanning Lu, Tuan Ling Neo, Ding Xiang Liu, and James P. Tam; Importance of SARS-CoV spike protein Trp-rich region in viral infectivity; Biochemical and Biophysical Research Communication; 2008 July; https://dx.doi.org/10.1016%2Fj.bbrc.2008.04.0444.

[79]. Ying Liao , Si Min Zhang, Tuan Ling Neo & James P Tam; Tryptophan-dependent membrane interaction and hetero-merization with the internal fusion peptide by the membrane proximal external region of SARS-CoV spike protein; Biochemistry ; 2015 March; https://doi.org/10.1021/bi501352uu.

[80]. Megan W. Howard, Emily A. Travanty, Scott A. Jeffers, M. K. Smith, Sonia T. Wennier, Larissa B. Thackray and Kathryn V. Holmes; Aromatic amino acids in the juxtamembrane domain of severe acute respiratory syndrome corona-virus spike glycoprotein are important for receptor-dependent virus entry and cell-cell fusion; Journal of Virology; 2008 March; https://dx.doi.org/10.1128%2FJVI.01805-077.

[81]. Hao Xu, Liang Zhong, Jiaxin Deng, Jiakuan Peng,Hongxia Dan, Xin Zeng, Taiwen Li and Qianming Chen; High expression of ACE2 receptor of 2019-nCoV on the epithelial cells of oral mucosa; International Journal Oral Science; 2020 Feb; https://dx.doi.org/10.1038%2Fs41368-020-0074-xx.

[82]. Lili Chen, Jiajia Zhao, Jinfeng Peng, Xiaoshuang Li, Xuliang Deng, Zhi Geng , Zhenyu Shen, Fengyuan Guo, Qianwen Zhang, Yang Jin, Lin Wang & Songlin Wang ; Detection of SARS-CoV-2 in saliva and characterization of oral symptoms in COVID-19 patients; Cell Proliferation; 2020 October; https://doi.org/10.1111/cpr.129233.

[83]. Jian Fan, Fei Yu, Xiang Wang, Qianda Zou, Bin Lou, Guoliang Xie, Xianzhi Yang, Weizhen Chen, Qi Wang, Dan Zhang, Ruonan Wang, Baihuan Feng, Yuejiao Dong, Li Huang, Yun Teng, Zhenzhen Deng, Ling Yu,e Kaijin Xu, Jifang Sheng, Shufa Zheng, and Yu Chen; Hock-a-loogie saliva as a diagnostic specimen for SARS-CoV-2 by a PCR-based assay: A diagnostic validity study; Clinica Chimica Acta; 2020 December; https://doi.org/10.1016/j.cca.2020.10.0044.

[84]. Gregory W. Auner, S. Kiran Koya, Changhe Huang, Brandy Broadbent, Micaela Trexler, Zachary Auner, Angela Elias, Katlyn Curtin Mehne & Michelle A. Brusatori; Applications of Raman spectroscopy in cancer diagnosis; Cancer and Metastasis Reviews; 2018 Decembe; https://doi.org/10.1007/s10555-018-9770-99.

[85]. S. Nie and S. R. Emory; Probing Single Molecules and Single Nanoparticles By Surface-Enhanced Raman Scattering; Science; 1997; DOI: 10.1126/science.275.5303.1102.

[86]. M.R.K. Ali, B. Snyder and M.A. El-Sayed; Synthesis And Optical Properties Of Small Au Nanorods Using Seedless Growth Technique; Langmuir; 2012.

[87]. M.C. Daniel and D. Astruc; Gold Nanoparticles: Assembly, Supramolecular Chemistry, Quantu Size-Related Properties and Applications To-ward Biology, Catalysis, And Nanotechnology; Chemistry Review; 2004.

[88]. E. C. Dreaden, A. M. Alkilany, X. Huang, C.J. Murphy, and M. A. El-Sayed; The Golden Age: Gold Nanoparticles For Biomedicine; Chemistry Soc. Rev.; 2012.

[89]. SEM and TEM micrographs of laser irradiated various shaped colloidal SERS Au nanoparticles; https://www.intechopen.com/media/chapter/57501/media/ F3.png.

[90]. Surface-enhanced Raman spectroscopy coupled with Gold nano-particles; https://www.google.com/url?sa=i&url=https%3A%2F%2Fwww.sciencedirect.com%2Fscience%2Farticle%2Fpii%2FS0956713516301724&psig=AOvVaw2m5L3U3XmPvutMNT0lphs1&ust=1630916902885000&source=images&cd=vfe&ved=0CAsQjRxqFwoTCMCPmaC15_ICFQAAAAAdAAAAABAD.

[91]. D. R. Monteiro, L. F. Gorup, S. Silva, M. Negri, E. R. Camargo, R. Oliveira, D. B. Barbosa and M. Henriques; Silver Colloidal Nanoparticles: Antifungal Effect Against Adhered Cells And Biofilms Of Candida Albicans AndCandida Glabrata; Biofouling; 2011.

[92]. Andressa M. Kubo , Luiz F. Gorup , Leonardo Toffano , Luciana S. Amaral , Edson Rodrigues-Filho , Haider Mohan , Ricardo Aroca and Emerson R. Camargo, Nanostructured Assemblies of Gold and Silver Nanoparticles for Plasmon Enhanced Spectroscopy Using Living Biotemplates; 2017.

[93]. J M McLella, A Siekkinen, J Chen, Y Xia; Comparison of the surface-enhanced Raman scattering on sharp and truncated silver nanocubes; Chemical Physics Letters; 2006.

[94]. TANUJJAL BORA; Recent Developments on Metal Nano-particles for SERS Applications; IntechOpen; 2017 December; http://dx.doi.org/10.5772/intechopen.71573 .

[95]. Khalid Alaqad and Tawfik A Saleh; Gold and Silver Nanoparticles: Synthesis Methods, Characterization Routes and Applications towards Drugs; Journal of Environmental & Analytical Toxicology; 2016.